REPORT DOCUMENTATION PAGE

AFRL-SR-AR-TR-03-

0376

1. AGENCY USE ONLY *(Leave blank)*

2. REPORT DATE

3. REPORT TYPE AN

15 Mar 99 - 14 Mar 2003 Final Report

4. TITLE AND SUBTITLE

(DEPSCOR 99) Molecular Beam Epitaxy of Nitridel: Theoretical Modeling and Process Simulation

5. FUNDING NUMBERS

61103D
3484/BS

6. AUTHOR(S)

Dr Venkat

7. PERFORMING ORGANIZATION NAME(S) AND ADDRESS(ES)

University of Nevada Las Vegas
4505 Maryland Parkway
Las Vegas NV 89154

8. PERFORMING ORGANIZATION REPORT NUMBER

9. SPONSORING/MONITORING AGENCY NAME(S) AND ADDRESS(ES)

AFOSR/NE
4015 WILSON BLVD
SUITE 713
ARLINGTON VA 22203

10. SPONSORING/MONITORING AGENCY REPORT NUMBER

F49620-99-1-0188

11. SUPPLEMENTARY NOTES

12a. DISTRIBUTION AVAILABILITY STATEMENT

APPROVED FOR PUBLIC RELEASE, DISTRIBUTION UNLIMITED

12b. DISTRIBUTION CODE

13. ABSTRACT *(Maximum 200 words)*

A rate equation approach is proposed based on physically sound surface processes to investigate the molecular beam epitaxy growth and doping of of 111-N using ammonia and ECR plasma source. A surface riding layer of Ga/In/Mg and ammonia or N plasma species arc included in the model. The surface riding species are allowed to undergo several physical and chemical processes. In the case of ammonia, the simulated Ga incorporation rate as a function of ammonia pressure and substrate temperature are in excellent agreement with the experimental data. Ga incorporation increases with increasing ammonia overpressure. Simulated Ga desorption parameter versus time data is also in good qualitative agreement with the experimenta data. In the case of ECR plasma, electron concentration obtained from bulk vacancy concentrations of Ga and N decreases linearly with ECR power unlike the experimental observation of exponential decrease.

In JnGaN growth, results of In incorporation obtained from simulations and experiments are in excellent agreement for various growth conditions. In segregation is found to be negligible below 580 "C. Above 640 "C, the segregation dominates the kinetics. This temperature dependeuce is found to be independent of the fluxes. In MgGaN growth, simulations were carried for various growth temperatures in the range of 600-750 "C.' with constant flux rates of Mg, Ga and N. For the given flux rates, it is found that Mg segregates to the surface with the increase in temperature. Above 750 "C a dopant depleted zone is formed below the surface layer. Results obtained from simulations are in excellent agreement with the experimental data.

14. SUBJECT TERMS

15. NUMBER OF PAGES

16. PRICE CODE

17. SECURITY CLASSIFICATION OF REPORT	18. SECURITY CLASSIFICATION OF THIS PAGE	19. SECURITY CLASSIFICATION OF ABSTRACT	20. LIMITATION OF ABSTRACT
UNCLASSIFIED	UNCLASSIFIED	UNCLASSIFIED	UL

Principal Investigator: Rama Venkat

Department of Electrical and Computer Engineering

University of Nevada, Las Vegas

Las Vegas, NV 89154

Office: (702) 895 1094

Fax: (702) 895 4075

Program Title: DEPSCOR 99

Proposal Title: Molecular Beam Epitaxy of Nitrides: Theoretical Modeling and Process Simulation

Grant Number: F49620-99-1-0188

Project Period: 3 March 1999-14 March 2004

Report Period: 3 March 1999-14 March 2004

AFOSR Program Manager: Dr. Gerald L. Witt

Physics and Electronics, Electronic Devices,

Components and Circuits

Project Summary

A rate equation approach is proposed based on physically sound surface processes to investigate the molecular beam epitaxy growth and doping of of III-N using ammonia and ECR plasma source. A surface riding layer of *Ga/In/Mg* and ammonia or N plasma species are included in the model. The surface riding species are allowed to undergo several physical and chemical processes. In the case of ammonia, the simulated *Ga* incorporation rate as a function of ammonia pressure and substrate temperature are in excellent agreement with the experimental data. *Ga* incorporation increases with increasing ammonia overpressure. Simulated *Ga* desorption parameter versus time data is also in good qualitative agreement with the experimental data. In the case of ECR plasma, electron concentration obtained from bulk vacancy concentrations of *Ga* and *N* decreases linearly with ECR power unlike the experimental observation of exponential decrease.

In *InGaN* growth, results of *In* incorporation obtained from simulations and experiments are in excellent agreement for various growth conditions. *In* segregation is found to be negligible below 580 ^{o}C. Above 640 ^{o}C, the segregation dominates the kinetics. This temperature dependence is found to be independent of the fluxes. In *Mg-GaN* growth, simulations were carried for various growth temperatures in the range of 600-750 ^{o}C with constant flux rates of *Mg*, *Ga* and *N*. For the given flux rates, it is found that *Mg* segregates to the surface with the increase in temperature. Above 750 ^{o}C a dopant depleted zone is formed below the surface layer. Results obtained from simulations are in excellent agreement with the experimental data.

TABLE OF CONTENTS

LIST OF TABLES

LIST OF FIGURES

1. RATE EQUATION MODEL

1.1.Surface Processes

The MBE growth simulation of *GaN*, *InGaN* on wurtzitic *GaN* substrate oriented along [0001] and *Mg* doping of wurtzitic *GaN* were considered. The dynamic processes occurring on a surface riding physisorbed material layer (PM) and the surface of the crystalline epilayer play a crucial role in the growth and composition of compound semiconductors. The atoms or molecules of this layer are physisorbed on to the surface by Vander Waals type of binding, i.e., weakly bonded to the surface.

Several dynamic processes such as the adsorption of atom onto the crystal, the evaporation of atom out of it and the segregation of atoms from the bulk into the PM layer are considered for the PM layer. These processes are assumed to be Arrhenius type and are given by:

$$\tau_i = \tau_{o,i,e} e^{\frac{E_i}{kT}} \tag{1}$$

where $\tau_{o,i,e}$ represents the time constant for the process i, E_i is the activation energy, k is the Boltzmann constant and T is the temperature in Kelvin.

The surface dynamic processes included for the epilayer are adsorption, evaporation, interlayer migration, intralayer migration and segregation. A schematic picture of these processes is shown in Figure 1 for *InGaN* and Figure 2 for *Mg-GaN*. Arrhenius type rate equations are assumed for the rate of evaporation and migration of atoms, and are given by:

$$R = R_o e^{\frac{-E_{act}}{kT}} \tag{2}$$

where R_o is the frequency prefactor, E_{act} is the activation energy, k is the Boltzmann constant and T is the temperature in Kelvin.

1.2. Time Evolution Equations

1.2.1. GaN using Ammonia

Nitride MBE growth involves the presence and dynamics of a physisorbed material (PM) state riding on the surface for the constituent elements, especially for the NH_3 molecule. Typically, these molecules/atoms form a weakly bound precursor state with Van der Waal type binding. This layer of material undergoes two dynamic processes, chemisorption into regular lattice sites and desorption out of the layer in to vacuum. The NH_3 molecules in the PM layer undergo the following chemical reaction by pyrolysis:

$$NH_3 + Ga\,(crystal\ surface) \Leftrightarrow GaN\,(crystal\ surface) + \frac{3}{2}H_2 \qquad (3)$$

1.2.2. *GaN* and *InGaN* Growths

The time evolution of the growing epilayer is described through the change of macro variables such as coverages of individual species resulting from the surface processes. The macro variables of growth are normalized with respect to the maximum number of possible atoms in the layer, and therefore have values between 0 and 1. Coverage is 1 when the layer is full and 0 when the layer is empty.

The layer coverages of *Ga*, *N*, and *In* in their respective layers are the macro variables describing the growth and are denoted as:

$C_{Ga}(2n)$: layer coverage of *Ga* in the 2nth layer,

$C_N(2n+1)$: layer coverage of *N* in the 2n+1th layer,

$C_{In}(2n)$: layer coverage of *In* in the 2nth layer,

C_{Ga}^{PM}, C_N^{PM} and C_{In}^{PM} :PM layer coverage of *Ga*, *N* and *In* respectively. (4)

where n is the layer index, with the *Ga* and *In* belonging to even numbered layers, and the *N* belonging to the odd numbered layers. Note that the coverages can have values between 0 and 1, depending on how full a layer is.

The time evolution of the layer coverage of *In* in the 2nth layer due to the various surface processes is given by:

$$\frac{dC_{In}(2n)}{dt} = \left([C_N(2n-1) - C(2n)] \times \left[J_{In} + \frac{C_{In,phy}}{\tau_{in}^{In}} \right] \right) \tag{A1}$$

$$+ [C_N(2n-1) - C(2n)] \times \left(R_0 e^{\frac{E_{d,In}(2n+2)}{kT}} \left(\frac{C_{In}(2n+2)}{C(2n+2)} \right) \right.$$

$$\times [C(2n+2) - C_N(2n+3)]$$

$$\left. + R_0 e^{\frac{E_{d,In}(2n-2)}{kT}} \left(\frac{C_{In}(2n-2)}{C(2n-2)} \right) \times [C(2n-2) - C_N(2n-1)] \right) \tag{B1}$$

$$- R_0 e^{\frac{E_{d,In}(2n)}{kT}} \left(\frac{C_{In}(2n)}{C(2n)} \right) \times [C(2n) - C_N(2n+1)]$$

$$\times ([C_N(2n+1) - C(2n+2)] + [C_N(2n-3) - C(2n-2)]) \tag{C1}$$

$$- R_0 e^{\frac{E_{e,In}(2n)}{kT}} \left(\frac{C_{In}(2n)}{C(2n)} \right) \times [C(2n) - C_N(2n+1)] \tag{D1}$$

$$-R_0 e^{\frac{E_{s,In}(2n)}{kT}}\left(\frac{C_{In}(2n)}{C(2n)}\right)\times[C(2n)-C_N(2n+1)] \qquad \text{(E1) (5)}$$

where the term A1 represents the increase in $C_{In}(2n)$, resulting from adsorption of *In* from the incoming flux. The rate of adsorption is the product of the available sites for *In* incorporation on the surface, $[C_N(2n-1)-C(2n)]$, and the fluxes of *In*, J_{In} from the molecular beam and $\frac{C_{In,phy}S_1}{\tau_{in}^{In}}$ from the PM layer. The sticking coefficient of *In* is taken as unity. The term B1 describes the increase in $C_{In}(2n)$ resulting from migration of *In* into the $2n^{th}$ layer from all the adjacent layers, i.e., $(2n+2)$ and $(2n-2)$. $[C(2n-2)-C_N(2n-1)]$ is the fraction of available sites for *In* in the $2n^{th}$ layer. *In* and *Ga* are the two possible elements in the cation sub-lattice. The total coverage of a cation layer, $C(2n+2)$, is given by:

$$C(2n+2)=C_{Ga}(2n+2)+C_{In}(2n+2) \qquad (6)$$

The fraction $\frac{C_{In}(2n+2)}{C(2n+2)}$ is used to include only the *In* portion of all the cations in the layer for migration. The activation energy for *In* diffusion in the $2n\text{-}2^{th}$ layer depends on the coverage of the layer and is given as:

$$E_{d,In}(2n-2)=E_{d,In,iso}+6E_{In,In}C_{In}(2n-2)+6E_{Ga,In}C_{Ga}(2n-2) \qquad (7)$$

where, $E_{d,iso}$ is the activation energy of isolated atoms, and the second neighbor atom-atom pair interaction energies, $E_{Ga,In}$ and $E_{In,In}$, with a factor of six for the maximum possible number of neighboring atoms. Thus, when the coverage is very small,

$E_{d,In}(2n-2)$ equals $E_{d,In,iso}$. $[C_N(2n)-C(2n+1)]$ is the portion of the nth layer available for diffusion of *Ga/In* from the neighboring layers. Term C1 represents the migration process opposite to that represented by the term B1. The terms D1 and E1 in Equation (4) describes the decrease in $C_{In}(2n)$ resulting from the evaporation and segregation of *In* atoms, respectively, from the 2nth layer. $\frac{C_{In}(2n)}{C(2n)}[C(2n)-C_N(2n+1)]$ represents the fraction of *In* in the 2nth exposed layer to the vacuum so that it is available for segregation or evaporation.

The descriptions of the activation energy for evaporation and segregation are similar to that of diffusion given by equation (5), except for the value for the isolated adatom. The equations are

$$E_{e,In}(2n) = E_{e,In,iso} + 6E_{In,In}C_{In}(2n) + 6E_{Ga,In}C_{Ga}(2n) \tag{8}$$

and

$$E_{s,In}(2n) = E_{s,In,iso} + 6E_{In,In}C_{In}(2n) + 6E_{Ga,In}C_{Ga}(2n) \tag{9}$$

for evaporation and segregation, respectively.

The time evolution of the layer coverage of *In* in the PM layer, $\frac{dC_{In}}{dt}$, is given by:

$$\frac{dC_{i,phy}}{dt} = \begin{aligned}&(J_i(1-S_1)) - \frac{C_{i,phy}}{\tau_{ev}^i} - \frac{C_{i,phy}S_1}{\tau_{in}^i} + R_0 e^{\frac{-E_s(2n)}{kT}}\left(\frac{C_{i,phy}(2n)}{C(2n)}\right)\\ &\times[C(2n)-C_N(2n+1)]\end{aligned} \tag{10}$$

where i represents *In* in this case and S_1 is the sum of all crystal sites that are available for the incorporation of species in the appropriate sub-lattice. J_i is the molecular flux of the ith species coming onto the substrate. The first term denotes the increase in PM coverage due to arrival of ith species flux. The second and third term denotes the net loss of PM layer

coverage due to evaporation and chemisorption. The last term denotes the gain in the PM layer coverage due to segregation.

A similar equation is written for physisorbed Ga and *N* without the segregation term and the *N* getting incorporated in the anion sub-lattice. As only monolayer coverage of the PM layer is effective in the surface dynamics, the sum of the coverage of *Ga*, *In* and *N* in the PM layer cannot exceed 1. R_0 is the frequency factor and $E_s(2n)$ is the activation energy for the segregation of the i^{th} species from the crystal surface to the PM layer. Equations similar to (4-9) are written for *N* and *Ga*, except that the term E, which represents segregation, is excluded from them.

The time evolution of the layer coverage of *Ga* in the $2n^{th}$ layer due to the surface processes is given by

$$\frac{dC_{Ga}(2n)}{dt} = \left(\left[C_N(2n-1) - C(2n) \right] \times \left[J_{Ga} + \frac{C_{Ga,phy}}{\tau_{in}^{Ga}} \right] \right) \tag{A2}$$

$$+ \left[C_N(2n-1) - C(2n) \right] \times \left(R_0 e^{\frac{E_{d,Ga}(2n+2)}{kT}} \left(\frac{C_{Ga}(2n+2)}{C(2n+2)} \right) \right.$$

$$\left. \times \left[C(2n+2) - C_N(2n+3) \right] \right.$$

$$\left. + R_0 e^{\frac{E_{d,Ga}(2n-2)}{kT}} \left(\frac{C_{Ga}(2n-2)}{C(2n-2)} \right) \times \left[C(2n-2) - C_N(2n-1) \right] \right) \tag{B2}$$

$$- R_0 e^{\frac{E_{d,Ga}(2n)}{kT}} \left(\frac{C_{Ga}(2n)}{C(2n)} \right) \times \left[C(2n) - C_N(2n+1) \right]$$

$$\times \left(\left[C_N(2n+1) - C(2n+2) \right] + \left[C_N(2n-3) - C(2n-2) \right] \right) \tag{C2}$$

$$- R_0 e^{\frac{E_{e,Ga}(2n)}{kT}} \left(\frac{C_{Ga}(2n)}{C(2n)} \right) \times \left[C(2n) - C_N(2n+1) \right] \tag{D2) (11}$$

The terms A2, B2, C2 and D2 are similar to A1, B1, C1 and D1 respectively.

The time evolution of layer coverage of *N* is given by:

$$\frac{dC_N(2n+1)}{dt} = \left([C(2n) - C(2n+1)] \times \left[J_N + \frac{C_{N,phy}}{\tau_{in}^N} \right] \right) \tag{A3}$$

$$+ [C(2n) - C(2n+1)] \times \left(R_0 e^{\frac{E_{d,N}(2n+3)}{kT}} \left(\frac{C_N(2n+3)}{C(2n+3)} \right) \right.$$

$$\times [C(2n+3) - C(2n+4)]$$

$$\left. + R_0 e^{\frac{E_{d,N}(2n-1)}{kT}} \left(\frac{C_N(2n-1)}{C(2n-1)} \right) \times [C(2n-1) - C(2n)] \right) \tag{B3}$$

$$- R_0 e^{\frac{E_{d,N}(2n+1)}{kT}} \left(\frac{C_N(2n+1)}{C(2n+1)} \right) \times [C(2n+1) - C(2n+2)]$$

$$\times ([C(2n+2) - C_{Ga}(2n+3)] + [C(2n-2) - C(2n-1)]) \tag{C3}$$

$$- R_0 e^{\frac{E_{e,N}(2n+1)}{kT}} \left(\frac{C_N(2n+1)}{C(2n+1)} \right) \times [C(2n+1) - C(2n+2)] \tag{D3) (12}$$

where the terms A3, B3, C3 and D3 are similar to A1,B1,C1 and D1 respectively.

For the *GaN* growth with ammonia and ECR plasma *N*, the *In* flux is set to zero and hence all the coverage equations for *In* become unnecessary.

1.2.3. *Mg-GaN* Growth

The model used to describe *Mg-GaN* growth is same as the one used for *InGaN* growth except for the equation representing the activation energy of *Mg* diffusion. All the equations in *InGaN* except equation (7) are employed in this model with the subscript *In* changed to *Mg*.

The activation energy for *Mg* diffusion in the 2n-2th layer depends on the coverage of the layer and is given as:

$$E_{d,Mg,u}(2n-2) = E_{d,Mg,iso,u} + 6E_{Mg,Mg}C_{Mg}(2n-2) + 6E_{Ga,Mg}C_{Ga}(2n-2)$$

and

$$E_{d,Mg,d}(2n-2) = E_{d,Mg,iso,d} + 6E_{Mg,Mg}C_{Mg}(2n-2) + 6E_{Ga,Mg}C_{Ga}(2n-2) \qquad (13)$$

where, $E_{d,iso,u}$ is the activation energy of isolated atoms moving upwards and $E_{d,iso,d}$ is the activation energy for atoms moving downwards, and the second neighbor atom-atom pair interaction energies, $E_{Ga,Mg}$ and $E_{Mg,Mg}$, with a factor of six for the maximum possible number of neighboring atoms. Thus, when the coverage is very small, $E_{d,Mg}(2n-2)$ equals $E_{d,Mg,iso}$. $[C_N(2n) - C(2n+1)]$ is the portion of the nth layer available for diffusion of *Ga/Mg* from neighboring layers. The differentiation made here for *Mg* migrating up or down is not done for *In* migration as described in section 1.2.2.

1.3 Computational details and model parameters

Three first order nonlinear differential equations are required for the description of the evolution of each bilayer of *InGaN/Mg-GaN* with one equation describing the time evolution of each of the normalized macro-variables. Three additional equations are required for describing the time evolution of the PM layer. For this work, a total of 243 coupled nonlinear first order differential equations are required to solve the simultaneous growth of 80 bilayers and the PM layer.

Fourth order Runge-Kutta method was used to integrate the system of equations with time steps of less than 10^{-6} s to compute the values of each of the macro-variables as

a function of time for a growth time of 40 s. Similarly the activation energies for *In*, *Ga* and *N* evaporation process from the PM layer, E_{ev}^{In}, E_{ev}^{Ga} and E_{ev}^{N} respectively for *InGaN* and E_{ev}^{Mg}, E_{ev}^{Ga} and E_{ev}^{N} for *Mg-GaN* are assumed to be linearly dependent on their own coverage in the physisorbed layer [Table I].

In the case of *InGaN*, in order to make the model simple, the 2^{nd} neighbor interaction energies are kept the same and also the 1^{st} neighbor interaction energy between III-V atoms are kept identical. In *Mg-GaN* the first neighbor interaction energy between *Ga-N* and *Mg-N* are made equal. The first neighbor interaction energy between *Mg-Ga* is made smaller and is equal to the second neighbor interaction energies.

The prefactor of time constants for incorporation and evaporation processes are obtained according to the Arrhenius equation and related to the activation energies. The evaporation, segregation and diffusion processes in the surface of the epilayer are assumed to be thermally activated and are modeled with the frequency factor, R_0 and activation energy. R_0 is linearly dependent on the substrate temperature, and is given by:

$$R_0 = 2.08 \times 10^{10} \times T \tag{14}$$

This is based on the phonon frequency obtained using the equipartition energy principle. The frequency prefactor of diffusion processes are assumed constants. The frequency prefactor for segregation is considered to be linearly dependent on the substrate temperature, and is given by:

$$R_{0,s} = 1.743 \times 10^{10} \times T \tag{15}$$

The segregation process from the PM layer is allowed only for *In* in the *InGaN* and only for *Mg* in *Mg-GaN*. It is noted that $R_{0,s}$ is smaller than the R_0 of evaporation and diffusion. The frequency factors for the other processes are:

$R_0^{d,Ga}$ frequency factor for N for diffusion 4.38×10^7/s

$R_0^{d,N}$ frequency factor for Ga for diffusion 2.4×10^8/s.

$R_0^{d,In}$ and $R_0^{d,Mg}$ frequency factor for In and Mg for diffusion 4.38×10^5/s. (16)

1.4. Conversion among various flux units

The flux rates given in $atoms/cm^2 s$ are converted to $\left(\frac{ML}{s}\right)$. The conversion is done by multiplying the flux in $atoms/cm^2 s$, with the *area/site* of the wurzitic structure.

$$J\left(\frac{ML}{s}\right) = J\left(\frac{atoms}{cm^2 s}\right) \times \frac{\sqrt{3}}{2} a^2, \tag{17}$$

where a is the lattice constant. For GaN $a = 3.189 A^o$ and hence,

$$J\left(\frac{ML}{s}\right) = 8.8072 \times 10^{-16} \times J\left(\frac{atoms}{cm^2 s}\right) \tag{18}$$

For the wurzitic structure c = 5.185 A^o and every monolayer is equal to $\frac{c}{2}$ and hence,

$$J\left(\frac{ML}{s}\right) = \frac{J\left(\frac{nm}{\min}\right)}{\frac{c}{2}\left(\frac{nm}{\min}\right)} \tag{19}$$

2. RESULTS AND DISCUSSIONS

2.1. Ammonia as the Source

Two sets of growth conditions, one following the experiments of Held et. al.. [18] and the other following Jenny et. al. [2] were employed. The growth direction was [100]

for both the sets. In the case of Held et. al.. [1], the temperature was in the range of 1013-1113 K; NH_3 pressure, P_{NH_3}, was in the range of 0 -4.0×10^{-5} torr and Ga flux rate, J_{Ga} was in the range of 0 – 2.8 ML/sec. In the case of Jenny et. al. [2], the temperature was 1023 K; NH3 pressure, P_{NH_3}, was the range of 0 - 15.0 $\times10^{-7}$ torr and Ga flux rate, J_{Ga} was 0.14 ML/sec. P_{NH_3} was converted to a flux rate, J_{NH_3}, using the following equation:

$$J_{NH_3} = \frac{P_{NH_3}}{\sqrt{2\pi m k_B T}} \tag{20}$$

where m is the molecular weight of the NH_3 molecule, k_B is the Boltzmann constant and T is the source temperature.

Ga incorporation rate was obtained by time averaging Ga layer coverage for the entire growth period. A plots of Ga incorporation rate (ML/sec.) versus P_{NH_3} (torr) at constant Ga fluxes of 0.5 ML/sec. and 1.0 ML/sec. at the temperature of 1058 K is shown in Figure 3 for the growth conditions of Held et. al.. [1] along with their experimental data. The agreement between the results is excellent for the experimental values of Ga flux 1.0 ML/sec. case. In Figure 3, the vertical line clearly separate the pressures into two regimes with P_{NH_3}, less than 2.5 $\times10^{-5}$ torr (left of the line) representing the NH_3-limited regime and P_{NH_3} more than 2.5 $\times10^{-5}$ torr (right of the line) representing the Ga-limited regime. It is found that the *Ga* incorporation rate is linear in the NH_3 reaction-limited regime. In this regime, the excess Ga rides on the surface and reevaporates from the PM layer with activation energy of approximately 0.2eV.

A plot of *Ga* incorporation rate (ML/sec.) versus temperature is shown in Figure 4 for the growth conditions of Held et. al.. [1] along with their experimental data. The agreement between the results are excellent for most temperature values for a growth rate of 1.0 ML/sec.. The incorporation rate increases with temperature till 1093 K and then decreases. This behavior is due to competition between two thermally activated processes, the NH_3 reaction given by equation (3) and the reevaporation of Ga from the surface through the PM layer. The plots *Ga* incorporation rate versue temperature for Ga fluxs of 0.5 ML/sec., 1.5ML/sec., and 2.0 ML/sec. from simulation are also shown in Figure 4. It is noted that the temperature at which the growth rate peaks increases with the growth rate due to unavailability of surface *Ga* for evaporation and less residence time.

Growth rate versus *Ga* flux rate from our simulation is shown in Figure 5 along with experimental results of Held et. al.. [1]. The growth rate is *Ga*-limited with nearly unity incorporation up to a certain *Ga* flux, then the growth rate is NH_3-limited for higher *Ga* fluxes. In the NH_3-limited range, the growth rate reduces with *Ga* flux. The agreement between the results is excellent at low and high *Ga* flux rate. The simulation results deviate from experiments in the intermediate flux rate. The reason for this discrepancy is not clear. The reason for our observation is as follows. As the *Ga* flux rate increases, the proportion of *Ga* in the PM layer increases as shown in Figure 6. At the same time, the NH_3 proportion decreases as $C_{Ga,phy}+C_{NH_3,phy} \leq 1.0$. As the $C_{NH_3,phy}$ decreases, the incorporation rate of *N* decreases and hence the growth rate decreases.

The Ga incorporation rate (ML/sec.) as a function of temperature for several *Ga* / NH_3 flux ratios is shown in Figure 7. For this set of data, the ratio was fixed and the

temperature was varied. Even though the experimental [3] and simulation results are in the same approximate range, they do not agree either qualitatively or quantitatively. The trend seems similar. The reason for the discrepancy is not clear.

Desorption rate of Ga, D_{Ga}, was found as the difference between the arriving atoms and the change in the total atom concentration in the crystal and the PM layer in a preset short period of time. Mathematically, it can be written as:

$$D_{Ga} = J_{Ga}\Delta t - \sum_{all-layer}[C_{Ga}(2n)(t+\Delta t) - C_{Ga}(2n)(t)] - [C_{Ga,phy}(t+\Delta t) - C_{Ga,phy}(t)] \quad (23)$$

where Δt was arbitrarily chosen as 0.1 sec. A plot of *Ga* desorption rate computed using equation (23), D_{Ga} versus time for a NH_3 pressure of 2.95×10^{-7} torr is shown in Figure 8. The Ga flux was on from 10 to 20 seconds and at 20 seconds, the *Ga* flux was terminated. The *Ga* desorption rate initially increases rapidly and reaches a steady state within 3 sec. After the *Ga* flux is terminated, the *Ga* desorption flux decreases exponentially to zero in 3 sec. There are two components to the desorption process, one from the surface riding Ga and the other from the crystal with activation energies of 0.2 eV and 2.54 eV (isolated adatom), respectively. This behavior is in qualitative agreement with the results of Jenny et. al.[2] and Held et. al.. [1]. Quantitative comparison is not possible due to the arbitrary units of the experimental data.

GaN growth using NH_3 involves competition between NH_3 pyrolysis and *Ga* reevaporation, which are both thermally activated. For every set of *Ga* flux and P_{NH_3}, there is an optimum temperature for maximum *Ga* incorporation. This value of maximum incorporation rate can be less than either the *Ga* flux rate for *Ga* limited case or the *N* incorporation rate for ammonia reaction limited case, depending on the growth

conditions. For a given growth temperature and *Ga* flux, the *Ga* incorporation rate saturates beyond a particular NH_3 pressure. *Ga* reevaporation has two components, one from the PM layer and the other from the surface of the crystal.

Additionally, it is clear from the discussion related Figure 4 there is an additional competition between the species occupying the PM layer, i.e. *Ga* and NH_3. Thus competition decides the proportion of each species in the layer, which, in term, decides the dynamics of growth and growth rate.

For the growth conditions studied, the practical lower limit for ammonia decomposition appears to be 973 K. In general, the ammonia reaction rate increases with temperature as it is thermally activated. The ammonia decomposition can change with substrate, polarity, and growth condition, even though in this study, the influence of substrate type, orientation and polarity are not studied. The surface polarity will influence the growth kinetics, but in our model, this influence gets embedded indirectly in the fitted model parameters.

2.2. Modified Rate Equation Model for Growth of *GaN* using ECR Plasma

The operation of an ECR source is extremely complex and characterized by a strong coupling of various physical and chemical phenomena: power coupling, magnetic field-microwave interaction, plasma generation, plasma heating, rarefied gas flow, generation and transport of active species, and interaction of various species with walls and wafers. Thus, kinetic models such as particle in cell techniques to study the physics of plasma sources are extremely complex. Recently, simple zero-dimensional models

have been used to analyze high-density plasma used in processing applications [4,5]. In this chapter, a brief discussion of the zero-dimensional model of Meyyappan et. al.. [4,5] for ECR plasma simulation is presented. The parameters required for the model and results of the ECR simulation program, SAMPR [4,5] are also discussed. Finally, the results from the SAMPR are used in our MBE growth model.

A zero-dimensional model simply consists of balance equations for total mass, mass of various neutral and ionic species, and gas energy along with a plasma power (energy) balance equation. A Mass balance is considered for each of the neutral and ionic species in the plasma and accounts for changes due to flow balance due to flow, creation, and annihilation reactions. In addition to mass balance, power balance is also considered.

The possible nitrogen species considered are N_2^*, N_2^+, N ...etc. The simplicity of the approach does not permit investigation of microwave magnetic field interaction and related details; rather, the ECR power is just a lumped input parameter. The model provides volume-averaged densities of all species, gas, and electron temperatures. Obviously, no information on plasma uniformity or spatial profiles can be obtained from such a global model.

Electron impact, rotational, vibrational, and electronic excitation of N_2, ionization, dissociative ionization, and dissociation are included in this model. Neutral-neutral collisions have been ignored since the operating pressure in ECR devices is in the millitorr range. The wall collision of ions is assumed to liberate the corresponding neutral with a sticking probability of unity. The sticking coefficient for N atom recombination with stainless steel walls is taken to be 0.1.

ECR parameters similar to the ones used for experimental ECR-MBE growth [6] are employed for thus study. ECR plasma results from a systematic parametric study are presented to illustrate the effects of varying pressure, power, flow rate, and reactor dimensions. The operation range of ECR plasma parameters in summarized in Table II. The reactor dimensions correspond to a compact ECR source appropriate to fit onto a flange leading to the MBE growth chamber. It is assumed that the pressure and flow rate can be independently fixed at desirable values by adjusting the pumping speed. Note that the pressure is likely to vary along the length of the reactor under low pressure conditions (< 5mTorr), since the pressure drop required to push the required mass flow through the system may be large. Such a variation cannot be accounted for in the present analysis.

The active N volume density versus ECR power (W) and N_2 flow rate (sccm) is shown in Figure 9. The active nitrogen N density increases with both power and N_2 flow rate as expected. The flux of nitrogen atoms J_N is obtained by using the following equation:

$$J_N = f_{total-mass-flow} \times F_{nitrogen-mass-fraction} \times N_0 \times S_{sour-cross-section} \times M_{molecular-weight} \qquad (22)$$

where $f_{total-mass-flow}$ is the total mass flow, $F_{nitrogen-mass-fraction}$ is the nitrogen atom mass, N_0 is the Avagodro number, $S_{sour-cross-section}$ is the source cross sectional area and $M_{molecular-weight}$ is the molecular weight.

A plot of flux of active N versus ECR power (W) and flow rate of N_2 (sccm) is shown in Figure 10. The active N flux increases with both ECR power (W) and N_2 flow

rate (sccm). Since the flux is directly proportional to the density, which increases with both ECR, power and N_2 flow rate as shown in Figure 9.

The Rate Equation Model for growth of *GaN* using Ammonia is adopted directly for growth with ECR plasma. All of concepts, definitions, equations and parameters, physics and mathematics are the same. But the flux of N in the simulation program should replace that of NH_3. For ECR plasma, the fluxes of active nitrogen N can be obtained from ECR plasma source computer program SAMPR. Additionally, the PM layer equation, i.e, equation (10) should be replaced with a similar equation for active N.

The net electron concentration can be calculated using the following equation:

$$n_{electron-concentration} = 3n_{GaN}\sum[C_N(n) - C_{Ga}(n+1)]/n \qquad (23)$$

where n_{GaN} $(\sim 10^{23} cm^{-3})$ is a concentration of GaN at room temperature, $C_N(n)$ and $C_{Ga}(n+1)$ are the n^{th} layer coverage of N and $(n+1)^{th}$ layer of Ga, respectively, where n is constant. The reason for the 3 in equation (23) is that every Ga vacancy provides 3 electrons in crystal.

Plots of net electron concentration versus microwave power (W) for various flow rates are shown in Figures 11-13, respectively, for 973K, 1023K and 1073K along with the experimental results of Molnar et. al.. [6]. The experimental results of Molnar et. al.. [6] agree qualitatively with our results, but not quantitatively. With increasing ECR power, the active N flux increases and hence a decrease in the bulk N vacancies and the electron concentration. The dependence on the N_2 flow rate is very weak with higher

flow rate resulting in higher concentration. This is due to higher growth rate and hence less time for migration of both *Ga* and *N* at higher flow rate, which results in a greater Ga vacancy concentration. Figures 14-15 represents the *N* vacancy concentration versus temperature (K) and ECR power (W) for a different flow rate in a 3-D surface plot. The reason for poor quantitative agreement between the experiments with our results is as follows. Secondary ion msss spectrometry (SIMS) analysis of GaN films show that the concentration of Si, C, and O exhibit an experimental dependence as shown in Figure 17 [6]. Unfortunately, our ECR plasma model (SAMPR) does not capture this effect and our model does not allow for impurity incorporation. Films grown at high microwave power may have compensating centers due to impurities such as *C, O, Si* etc. Thus, our results cannot quantitatively agree with the experimental results of Molnar et. al.. [6].

Three-dimensions surface plots of growth rate ($\mu m / hr$) versus temperature (K) and ECR power (W) are shown in Figures 18-20, respectively, for flow rates of 3, 6, and 9 sccm. The general trend is the same in all three cases. The growth rate (below 1073 K) increases with temperature due to faster incorporation of active *N*, which is thermally activated. Beyond a critical temperature (large 1073 K), the growth rate decreases slightly due to evaporation of *Ga* directly from the crystal surface and from the floating *Ga* layer. This observation is confirmed by the there-dimensions surface plots of floating *Ga* (PM layer) against temperature and ECR power as shown in Figures 21-23, respectively, for flow rates 3 sccm, 6 sccm and 9 sccm. The growth rate is constant with ECR power as the growth condition already into *N* rich condition even with the lowest ECR power 18 W.

2.3. *In* segregration in *InGaN*

The model parameters employed for the simulation are reported in Table III. The growth conditions for the simulations were obtained from Averbeck *et.al.* [7]. The simulations were performed for two different nitrogen fluxes - 4.7*nm/min* and 12 *nm/min* and for the various temperatures in the range of 500-700 ^{o}C. The *In* content versus temperature plot shown in Figure 24 is obtained for the J_{Ga}/J_N ratio of 0.5 for various J_{In}/J_{Ga} ratios in the range of 0.33-3.0. The behavior of the plots is in qualitative agreement with the plots in Figure 1.a of Ref. [7]. It is found that for a given set of fluxes, below 580 ^{o}C, the fraction of *In* incorporated in to the layer closely follows the ratio of *In* flux to the total flux, i.e., J_{In}/J_{total}, and the percentage of Indium content in the layer is constant. Above 580 ^{o}C, the segregation phenomenon begins to dominate the kinetics due to increased thermal energy and hence, *In* content decreases with increasing temperature. Above 640 ^{o}C, only a trace of *In* is found in the growing layer. The active segregation energy of *In* is found from our simulation to be 2.9 *eV*, which is in close agreement with the segregation energy given in Ref. [7].

The *InN* loss as a function of temperature for various flux conditions is shown in Figure 24. The *InN* loss rate here is computed as the difference between the *In* flux and the incorporation rate of *In* and hence, includes both the loss of *In* due to segregation and the non-availability of *N* site. The simulations results show that for Group III rich conditions, the incorporation of Indium is limited by the nitrogen flux independent of the temperature. For *N*-rich growth conditions, at temperatures below 580 ^{o}C, the *InN* loss rate is insignificant as there is negligible segregation of *In* atoms due to lack of thermal

energy necessary for overcoming the segregation barrier. Above 640 ^{o}C, the loss rate attains a maximum value of the *In* flux, J_{In}. The results of Figure 24 and Figure 25 are consistent.

Plots of percentage of *Ga* content in the layer as a function of temperature for various fluxes are shown in Figure 26. At lower temperatures the incorporation of *Ga* governed by the ratio of J_{Ga}/J_{total}. At temperature above 640 ^{o}C the *Ga* content is 100%, as all *In* segregates to the surface. Thus, the results of Figure 24 and Figure 25 are in consistent with that of Figure 26.

Plots of growth rate versus temperature are shown in Figure 27 for various flux conditions. For J_N=4.7 *nm/min* and J_{In} / J_{Ga}=3.2, $J_{In} + J_{Ga}$ = 9.9 *nm/min.*, the growth rate was observed to be 3.2 *nm/min* at low temperatures and drops down to 1.6 *nm/min* at high temperatures. For J_N= 4.7*nm/min* and J_{In} / J_{Ga}=1.1, $J_{In} + J_{Ga}$ = 4.9*nm/min*, the growth rate is 2.5 *nm/min* at low temperatures and decreases to 1.6*nm/min.* for high temperatures. At low temperatures, *In* contributes to the growth rate in accordance to the flux ratio of *In* to *Ga*. At high temperatures, *In* segregates and hence the growth rate stays constant, irrespective of the ratio of *In* and *Ga* flux.

2.4. *Mg* Segregation in *Mg* doped *GaN*

The initial growth conditions are obtained from Myoung et. al. [6]. The flux of nitrogen and flux ratios as given in [6] were $8.3\times10^{14}\, atoms/cm.^2 s.$, $\left(\frac{J_{Ga}}{J_N}\right) \sim 0.13$ and $\left(\frac{J_{Ga}}{J_{Mg}}\right) \sim 2$ respectively. So the simulations are run for different temperatures in the

'range of 600-700 ^{o}C and at a particular flux rates of *Mg*, *Ga* and *N*, such as $5.5\times10^{13}\,atoms/cm^2s$, $1.1\times10^{14}\,atoms/cm^2s$ and $8.3\times10^{14}\,atoms/cm^2s$ respectively.

Plot of *Mg* dopant concentration versus layer number at 600 ^{o}C for various growth times are shown in Figure 28. For this plot, only layers that are full (i.e., $C_{Mg}+C_{Ga}=1$) after a particular time are considered. The temperature was kept constant at 600 ^{o}C. Plots were obtained for various time periods of growth in seconds. The peak value in each plot denotes the maximum surface concentration at that particular layer at a particular time. The values to the left of the peak point represent the bulk concentration and to the right represent the surface concentration. Initially *Mg* concentration at the surface close to the substrate is high and as the epilayers grow the surface concentration of the growing epilayer increases. *Mg* concentration at the surface close to the substrate decreases, which shows that there is a segregation of *Mg* from layer to layer.

Plot of Mg concentration versus layer number at 680 ^{o}C for various growth times is shown in Figure 29. Comparing Figures 26 and 27, it is observed that as the temperature increases, more and more *Mg* segregates to the surface and hence the bulk *Mg* concentration decrease with increase in temperature. This is in close agreement with the experimental results in Ref. [6].

Due to computational limitations, it is not possible to simulate growth of films of thickness ½ μm. Thus an extrapolated scheme was adopted which is described below.

A cubic curve fitting is obtained for a plot of particular temperature in order to obtain the maximum *Mg* concentration at various time periods of growth. Using the maximum *Mg* concentration obtained for various times, the constants a, b and c for the extrapolated equation

$$y_{\max}(t) = a\left(1 - e^{-bt}\right) + c \tag{24}$$

were obtained. Using equation (24), $y_{\max}(t)$ values were obtained for $t = 5$ minutes. The constants for the extrapolated maximum *Mg* surface concentration at various temperatures are listed in Table IV.

The extrapolated plot of maximum *Mg* surface concentration versus time is shown in Figure 30. The surface concentration increases with time and reaches a constant value, which implies that *Mg* segregates to the surface and saturates at a particular concentration. The result is in close agreement with Figure 1.a in Ref. [7]. The extrapolated *Mg* surface concentration versus thickness of the crystal from the substrate, for various growth temperatures, is shown in Figure 31. The surface concentration increases from the substrate and reaches a maximum at the surface of the crystal. Also the saturated *Mg* concentration increases with temperature and attains a peak value at 680 ^{o}C. Above 680 ^{o}C, the saturation value starts to decrease.

A plot of minimum and maximum *Mg* concentration versus temperature is shown in Figure 32. The minimum concentration implies the bulk *Mg* concentration and the maximum concentration implies the surface concentration. The bulk *Mg* concentration is obtained from the plots of dopant concentration versus layer number for various temperatures as shown in Figure 28 and 29. The point at which the plots start for various time periods is taken as the minimum bulk *Mg* concentration. At low temperatures the thermally activated segregation energy that aids in layer-to-layer segregation is not dominant. But as the temperature increases, segregation also increases. The surface concentration of *Mg* is a maximum at 680 ^{o}C. Results of Figure 32 are consistent with that of Figure 31.

When the temperature is raised above 750 ^{o}C there is a dip in the *Mg* concentration near the surface layer as shown in Figure 33. This region is called as dopant depleted zone. The rate of these migration from one layer to the other depends on the availability of *Mg* in the layers that are exposed to the vapor and the available sites in the layer to which the atoms migrate. For example, considering the n^{th} layer, the ratio of atoms migrating to the n^{th} layer to the atoms moving out of this layer is small. i.e. the rate of migration from the subsurface to the surface layer is larger than the rate of migration of atoms to the surface from the bottom layer. This gives rise to the deficiency of *Mg* atoms near the surface layer. The dip shown in 33 is in excellent agreement with the plots in Ref. [5, 6, 56].

3. CONCLUSIONS

A rate equation approach is employed to investigate the MBE growth of GaN using ammonia and ECR N plasma. A surface riding material layer of Ga/In/Mg and NH_3 along with the associated dynamics, incorporation of Ga and N in to the crystal and desorption are included in the model. Rates of all surface processes are assumed Arrhenius type. The simulated Ga incorporation rate as a function of ammonia pressure and substrate temperature is in excellent agreement with the experimental data [1]. Ga incorporation rate increases with increasing NH_3 overpressure and saturates at a maximum value at a large NH_3 overpressure. It clearly shows that the P_{NH_3} separates the growth regime into two areas: the Ga-limited and the NH_3-limited. It is found that the Ga incorporation rate is linear in the NH_3-limited and the excess Ga rides on the surface and

'reevaporates from the PM layer and the crystal surface. The Ga incorporation rate exhibits a peak at 1093 K due to competition between thermally activated pyrolysis of NH_3 and reevaporation of Ga from the surface. The growth regime is split into two parts in the Ga incorporation rate versus Ga flux rate behavior separated by at the peak incorporation rate: Ga-limited and NH_3-limited. There are some differences between the simulation results and the experimental results. The reason for our observation is that the NH_3 proportion in the PM layer decreases and results in the GaN growth rate decreases. The simulated Ga desorption parameter versus time is also in good agreement with the experimental data of Jenny et. al. [2].

The rate equation model was extended to ECR plasma MBE growth with necessary modifications. The growth conditions were kept identical to that used in the experiments of Ref [6]. The effect of the microwave power of the ECR plasma on the electron concentration was studied. The plots of the net electron concentration versus power (W) for various flow rates show that with increasing ECR power, the active N flux increases and hence the bulk N vacancies and the electron concentration decreases. It was found that the dependence of the election concentration on the N_2 flow rate is very weak that is due to the fact that the simulation growth conditions are in a high nitrogen regime. We investigated the influence of impurities in the GaN film growth at high microwave power. Plots of growth rate versus temperature and ECR power for various flow rates show the same general trend. The growth rate below 1073 K increases with temperature due to evaporation of Ga directly from the floating Ga layer and from the crystal surface. Under the N-rich condition, the growth rate is constant with ECR power.

The growth of *InGaN* and *Mg-GaN* by Molecular Beam Epitaxy is investigated with the rate equation model. The dependences of growth kinetics and *In/Mg* content on the temperature and flux conditions are analyzed using the simulation of the model. In the *InGaN* growth it is observed that the segregation phenomenon plays a major role in the surface kinetics and hence the *In* content of the grown layers. *In* segregation is found to be negligible below 580 ^{o}C. Above 640 ^{o}C, the segregation dominates the kinetics. This temperature dependence is found to be independent of the fluxes. In *Mg-GaN* growth, the phenomenon of segregation is justified with the simulation results and is in excellent agreement with the experimental results. The segregation of *Mg* is found to be dependant on the growth temperature. A dopant-depleted zone near the surface is observed during the growth at higher temperature. The observation is in qualitative agreement with the experimental data.

4. REFERENCES

1) R. Held et al., " In situ control of *GaN* growth by molecular beam epitaxy," J. Electron. Mater. 26, 272 (1997).

2) J. R. Jenny et al., "The effect *Al* on *Ga* desorption during gas source-molecular beam epitaxial growth of *AlGaN*," Appl. Phys. Lett. 72, 85 (1998).

3) R. Held et al., "A rate equation model for the growth of *GaN* on $GaN(000\bar{1})$ by molecular beam epitaxy," J. Appl. Phys. 87, 1219 (2000).

4) Meyyappan et al., "Modeling of electron cyclotron resonance discharges," IEEE Trans. Plasma Sci. 23, 623 (1995).

5) Meyyappan et al., "A spatially-averaged model for high density discharges," Vacuum 47, 215 (1996).

6) R. J. Molnar et al., "Growth of gallium nitride by electron-cyslotron resonance plasma-assisted molecular-beam epitaxy: the role of charged species," J. Appl. Phys. 76, 4587 (1994).

7) S. Guha, N. A. Bojarczuk, F. Cardone, "*Mg* in *GaN*: Incorporation of a volatile species at high temperatures during Molecular Beam Epitaxy", Appl. Phys. Lett., 71 (12), 1685, (1997).

8) J. M. Myoung, K. Kim, "Effects of growth temperature on *Mg*-doped *GaN* epitaxial films grown by plasma assisted Molecular Beam Epitaxy", J. Vac. Sci. Technol. A, 18 (2), 450, (2000).

9) T. S. Cheng, C. T. Foxon, N. J. Jeffs, D. J. Dewsnip, L. Flannery, J. W. Orton, S.V. Novikov, B. Ya Ber, Yu A. Kudriavtsev, "Studies of *Mg-GaN* grown by

MBE on GaAs(111)B substrates", MRS Internet J. Nitride Semicond., 2 (13), (1997).

10) J. M. Myoung, K. H. Shim, O. Gluschenkov, C. Kim, K. Kim, S. Kim, S. G. Bishop, "Effect of growth temperature on the properties of *p*-type *GaN* grown by plasma-assisted Molecular beam epitaxy", J. Cryst. Growth, 182, 241, (1997).

Table I. Fitted model parameters such as energies, time constants and frequency factors and their dependences for *GaN* growth.

Symbol	Description	Model Value
$\tau_{o,in}^{Phy,Ga}$	prefactor for physisorbed Ga incorporation	$1.6\times10^{-4}s$
$\tau_{0,in}^{Phy,N}$	prefactor for physisorbed N incorporation	$2.8\times10^{-12}s$
$\tau_{0,ev}^{Phy,Ga}$	prefactor for physisorbed Ga evaporation	$1000.0s$
$\tau_{0,ev}^{Phy,N}$	prefactor for physisorbed N evaporation	$3.5\times10^{-1}s$
$R_0^{d,Ga}$	frequency factor for Ga for diffusion	$2.4\times10^{8}/s$
$R_0^{d,N}$	frequency factor for N for diffusion	$4.38\times10^{7}/s$
E_{in}^{Ga}	activation energy for incorporation of Ga	$0.0eV$
E_{in}^{N}	activation energy for incorporation of N	$2.5eV$
E_{Ga-Ga}	2nd neighbor atom-atom pair interaction energy for Ga	$0.174eV$
E_{N-N}	2 neighbor atom-atom pair interaction energy for N	$0.190eV$
E_{Ga-N}	neighbor atom-atom pair interaction energy for Ga-N	$0.92eV$
$E_{d,iso}^{Ga}$	activation energy for diffusion for isolated Ga, atom	$1.2eV$
$E_{d,iso}^{N}$	activation energy for diffusion for isolated N atom	$1.2eV$
E_{ev}^{Ga}	activation energy for the Ga evaporation	$0.18+0.06C_{Ga}^{phy*}eV$
E_{ev}^{N}	activation energy for the N evaporation	$0.18+0.06C_{N}^{phy**}eV$

$*\,C_{Ga}^{phy}-Ga$ coverage in the physisorbed layer

$**C_{N}^{phy}-N$ coverage in the physisorbed layer

Table II. Operation range of ECR plasma parameters

Source radius r	1.27 cm
Source length L	10.00 cm
Nitrogen pressure	4.00 mtorr
ECR plasma power	18-25 W
N_2 flow rate	3-9 sccm

Table III. Parameters, their symbols and values used in the simulation. *X* represents *In* in *InGaN* and *Mg* in *Mg-GaN*

Symbol	Parameter Name	***InGaN* (eV)**	***Mg-GaN* (eV)**
$E_{X\text{-}X}$	2^{nd} neighbor atom-atom pair interaction energy for *X* cations.	0.08	0.08
$E_{Ga\text{-}Ga}$	2^{nd} neighbor atom-atom pair interaction energy for *Ga*	0.08	2.00
$E_{N\text{-}N}$	2^{nd} neighbor atom-atom pair interaction energy for *N*	0.08	0.08
$E_{Ga\text{-}X}$	1^{st} neighbor atom-atom pair interaction energy for *Ga-X*	0.08	0.08
$E_{Ga\text{-}N}$	1^{st} neighbor atom-atom pair interaction energy for *Ga-N*	2.0	2.0
$E_{X\text{-}N}$	1^{st} neighbor atom-atom pair interaction energy for *X-N*	2.0	2.0
$E_{d,iso,Ga}$	Activation energy for diffusion for isolated *Ga* atom	1.2	1.2
$E_{d,iso,N}$	Activation energy for diffusion for isolated *N* atom	1.2	1.2
$E_{d,iso,X}$	Activation energy for diffusion for isolated *X* cation atom	1.2	$E_{d,iso,u}$= 0.25 $E_{d,iso,d}$= 1.2
$E_{e,iso,Ga}$	Activation energy for evaporation for isolated *Ga* atom	6.24	12.0
$E_{e,iso,N}$	Activation energy for evaporation for isolated *N* atom	6.24	6.24
$E_{e,iso,X}$	Activation energy for evaporation for isolated *X* cation atom	6.24	6.24
$E_{ev,Ga}$	Activation energy for the physisorbed *Ga* evaporation	$0.18 + 0.06C_{Ga,phy}$	$0.18 + 0.06C_{Ga,phy}$
$E_{ev,N}$	Activation energy for the physisorbed *N* evaporation	$0.18 + 0.06C_{N,phy}$	$0.18 + 0.06C_{N,phy}$
$E_{ev,X}$	Activation energy for the physisorbed *X* cation evaporation	$0.18 + 0.06C_{X,phy}$	$0.18 + 0.06\ C_{X,phy}$
$E_{in,Ga}$	Activation energy for the *Ga* incorporation	0.0	0.0
$E_{in,N}$	Activation energy for the *N* incorporation	2.9	2.9
$E_{in,X}$	Activation energy for *X* cation incorporation	$0.5\ C_{X,\ phy}$	$0.5\ C_{X,\ phy}$
$E_{seg,\ X}$	Activation energy for X cation segregation	2.9	2.9

Table IV. Constants for the extrapolated maximum *Mg* concentration $y_{max}(t)$ at various temperatures.

Temperature (^oC)	a	b	c
600	-2.2e-04	4.6e-04	0.0336
625	-8.9e-05	4.8e-04	0.0223
650	-1.5e-03	2.0e-03	0.0511
675	-2.6e-04	8.4e-04	0.0288
680	-3.1e-04	9.0e-04	0.0288
700	-1.2e-03	1.7e-03	0.0511
725	9.3e-05	2.3e-04	0.0105

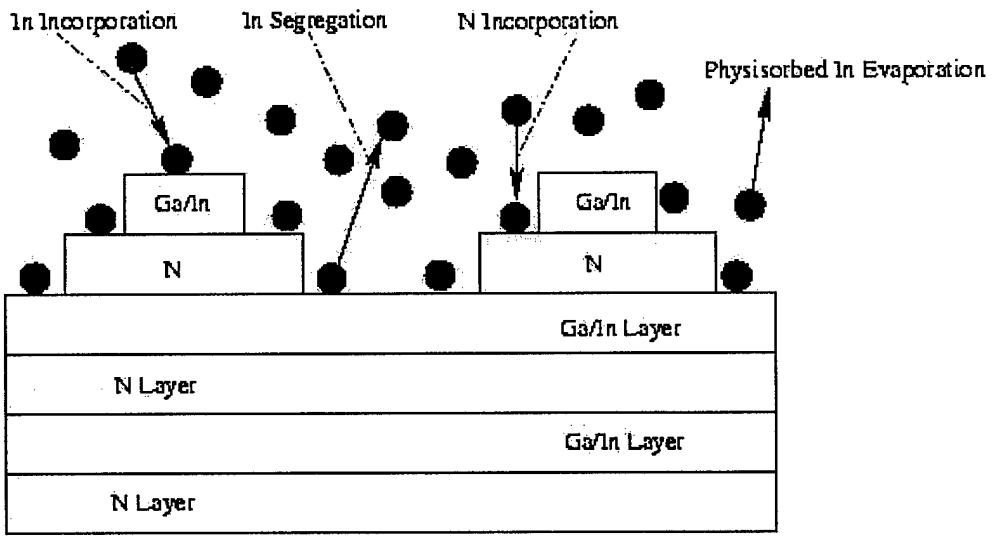

Figure 1. A schematic picture of the surface processes in MBE growth of *InGaN*

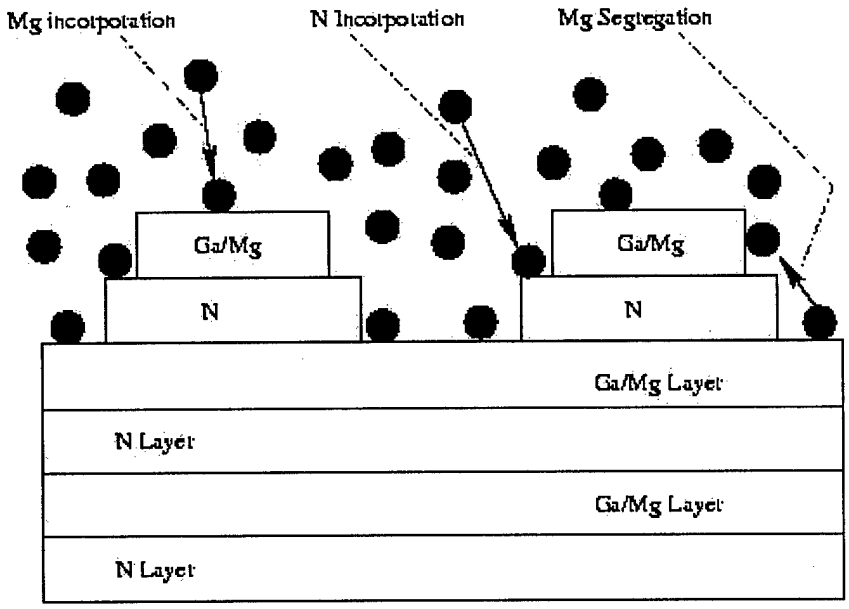

Figure 2. A schematic picture of the surface processes in MBE growth of *Mg-GaN*

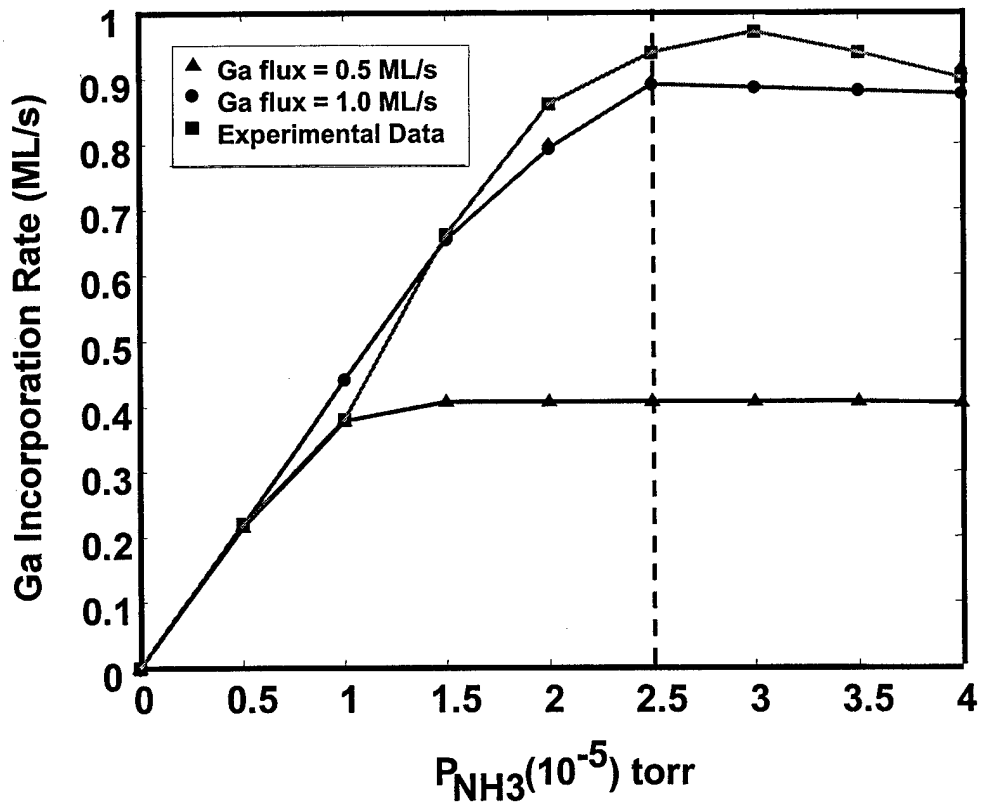

Figure 3. Simulation results of *Ga* incorporation coefficient versus NH_3 pressure along the experimental results of Held et. al.. [1].

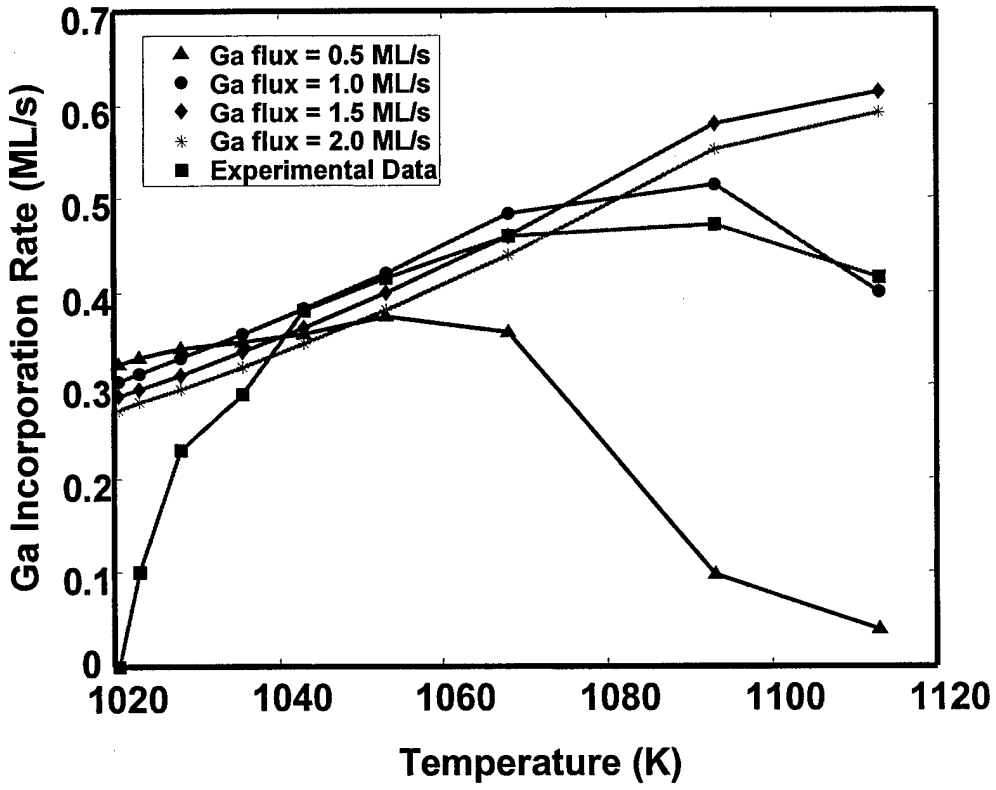

Figure 4. Simulation results of *Ga* incorporation coefficient versus substrate temperature along the experimental results of Held et. al.. [1].

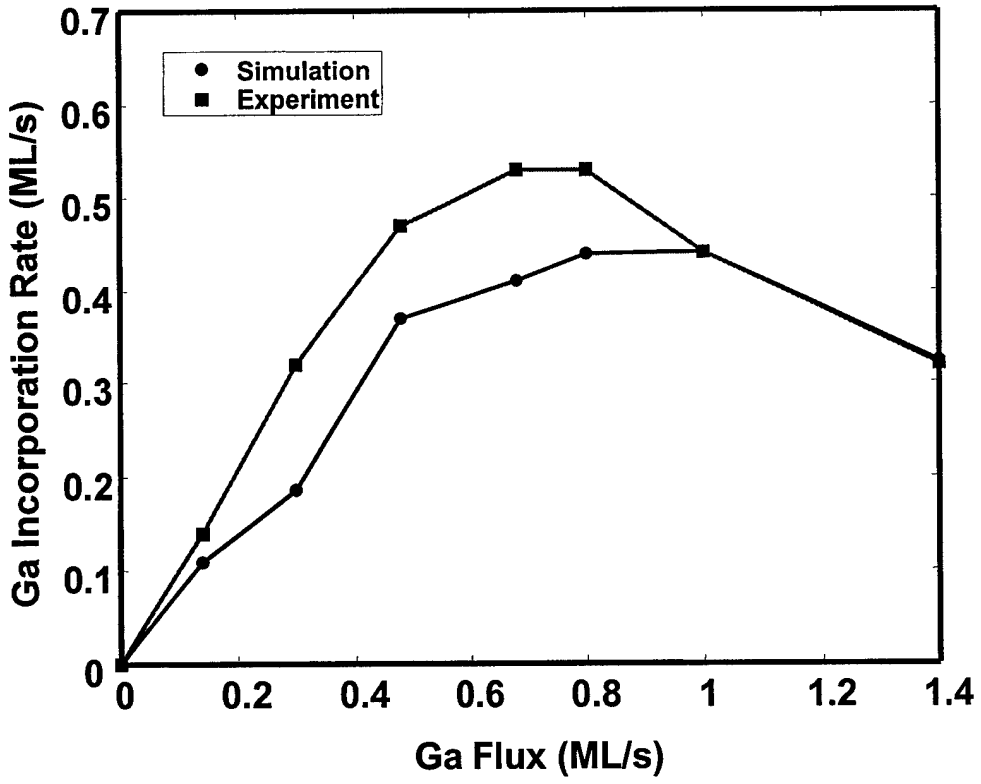

Figure 5. Simulation results of *Ga* incorporation coefficient versus *Ga* flux along the experimental results of Held et. al.. [1].

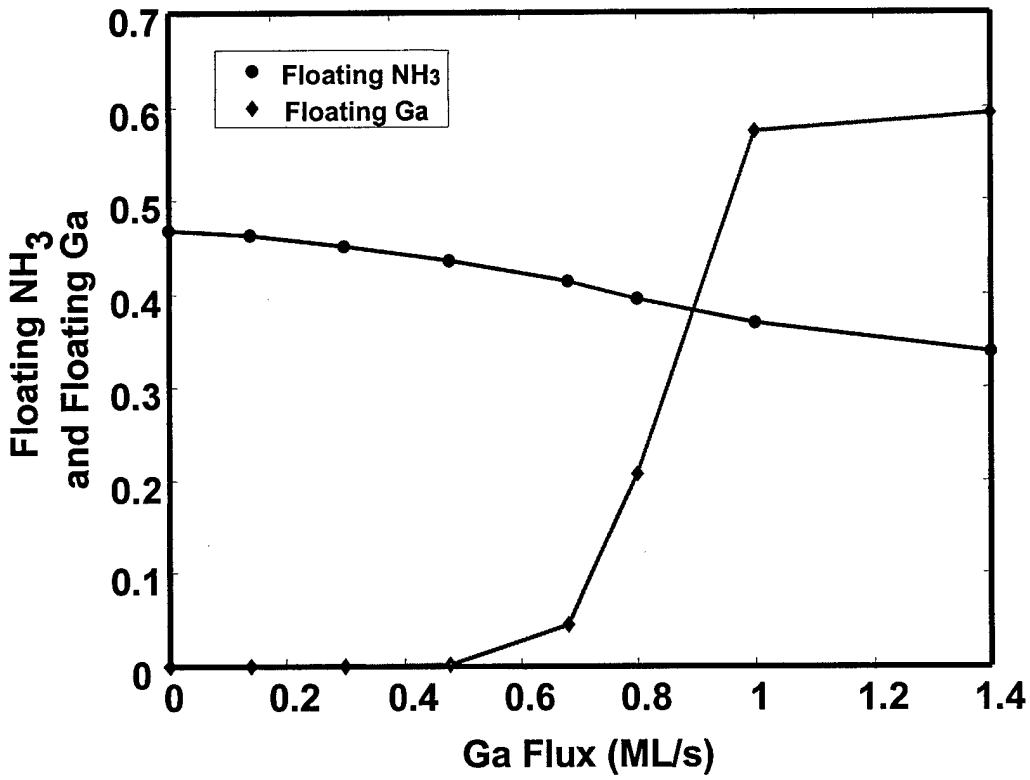

Figure 6. Simulation results of floating NH_3 and floating Ga versus Ga flux.

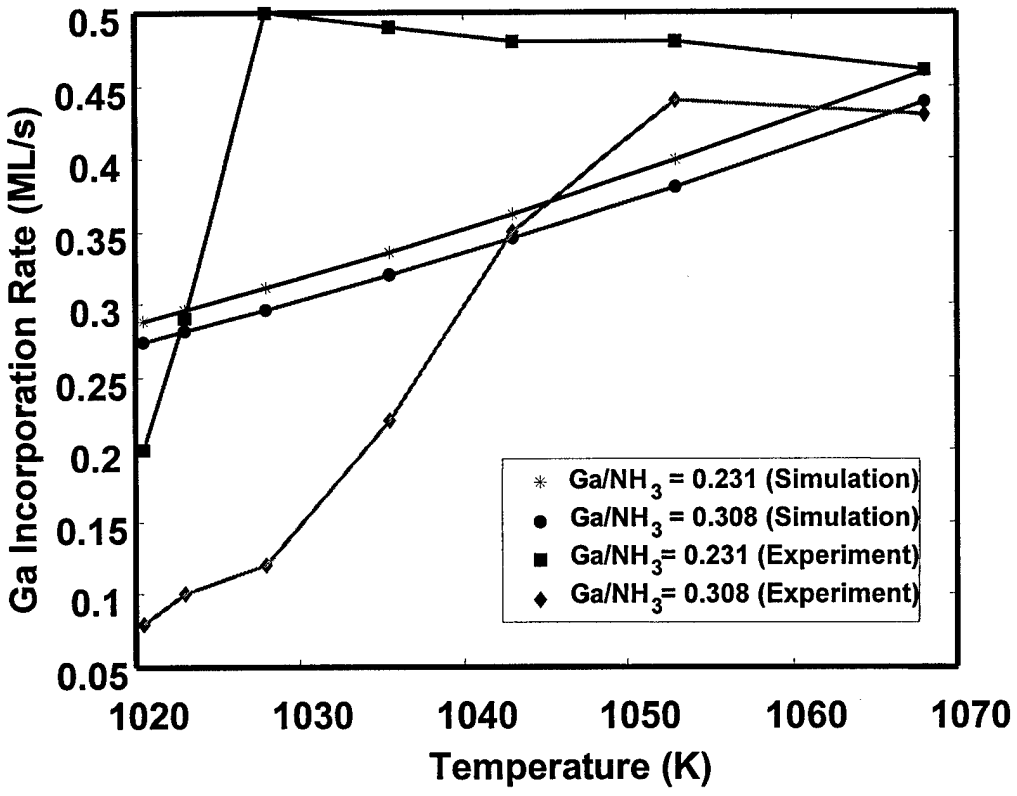

Figure 7. Simulation results of *Ga* incorporation coefficient versus substrate temperature for several Ga/NH_3 flux ratios along the experimental results of Held et. al.. [1].

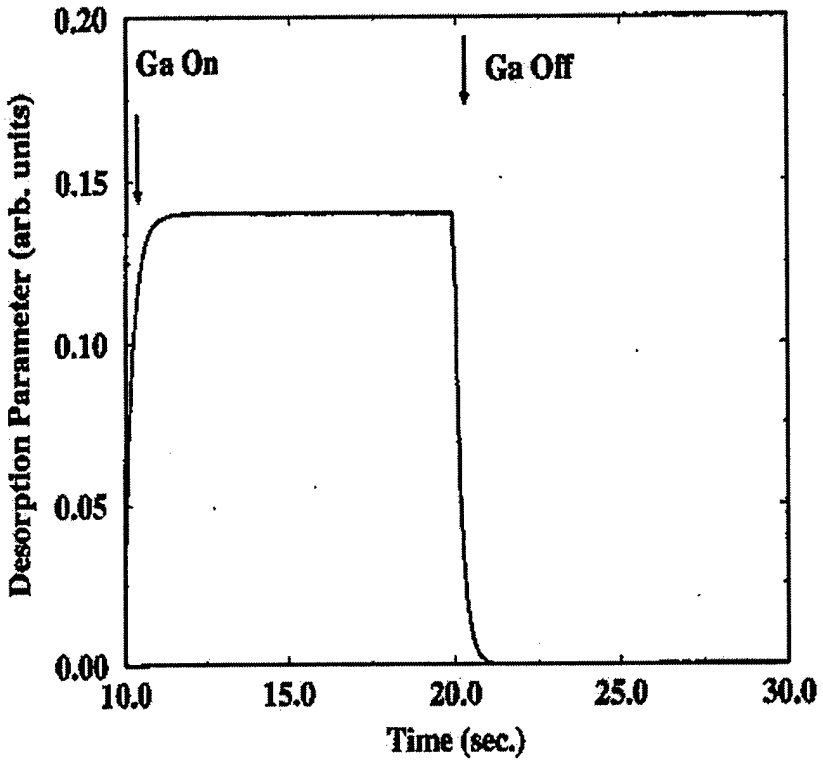

Figure 8. Simulation results of *Ga* desorption rate versus time for the growth conditions of Jenny et. al.. [2].

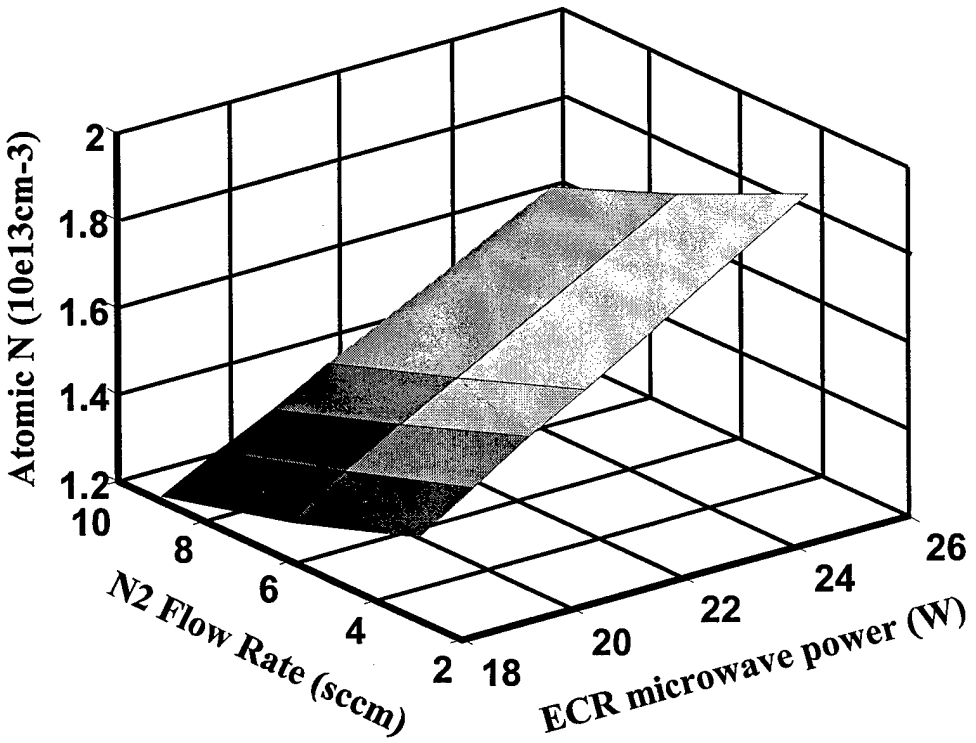

Figure 9. The dependence of atomic N concentration $(atoms/cm^3)$ on ECR power (W) and N_2 flow rate (sccm) at a temperature of 573 K .

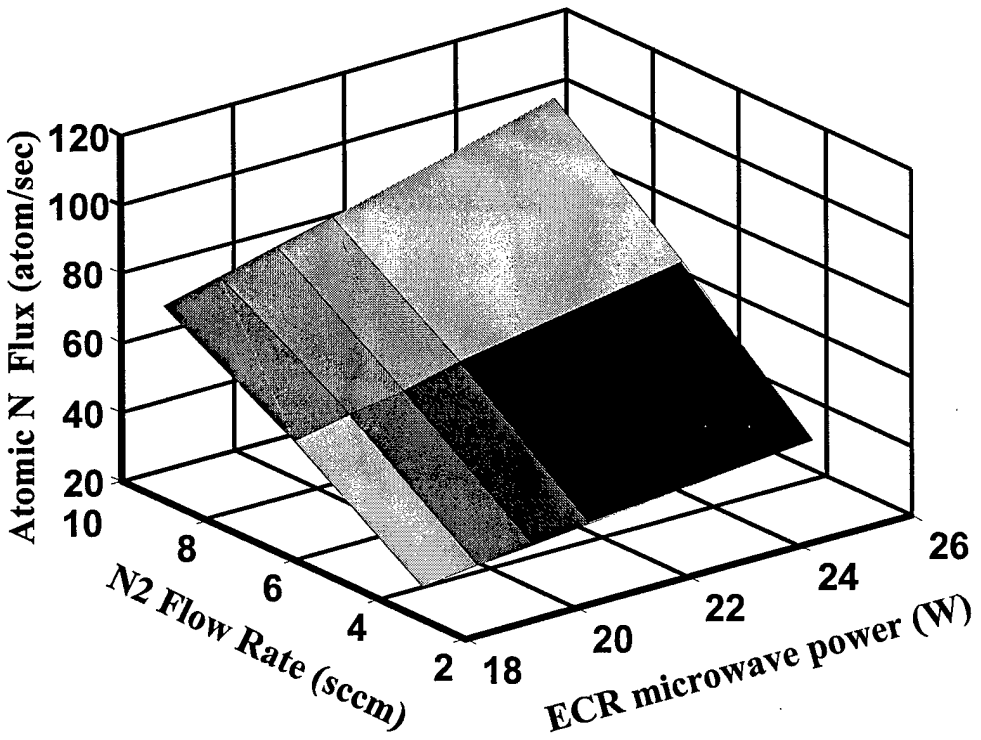

Figure 10. The dependence of atomic N flux ($atoms$/sec) on ECR power (W) and N_2 flow rate (sccm) at a temperature of 573 K.

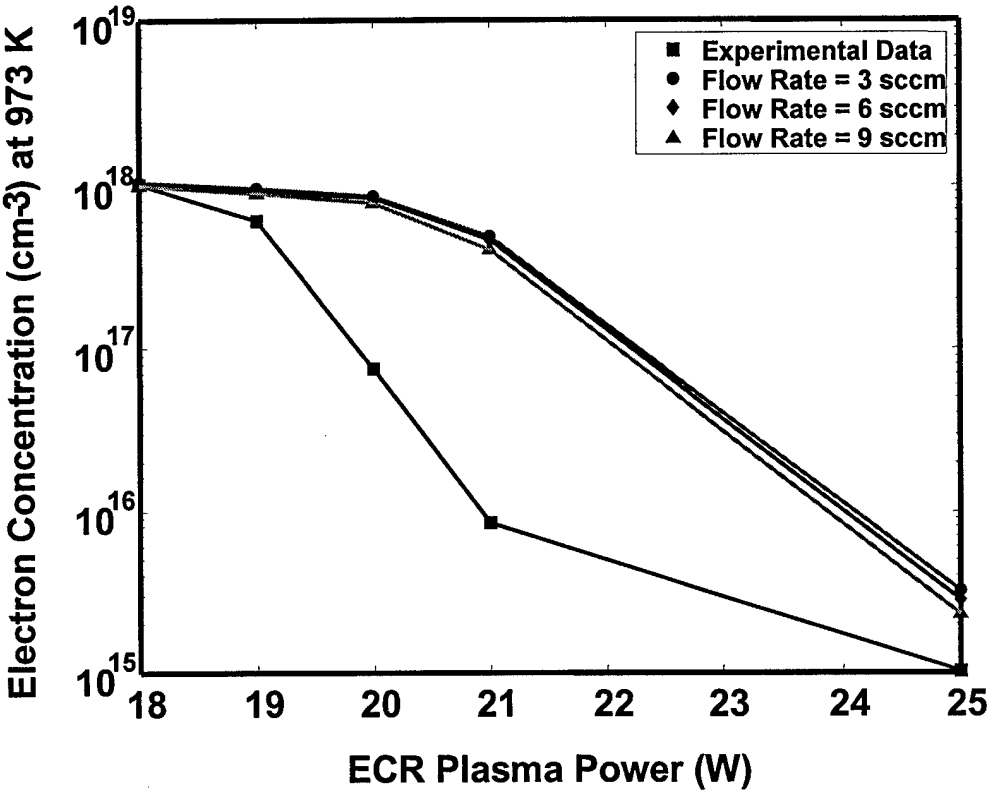

Figure 11. The variation of net electron concentration with the microwave power (W) at 973 K for various flow rates along with the experimental data [6].

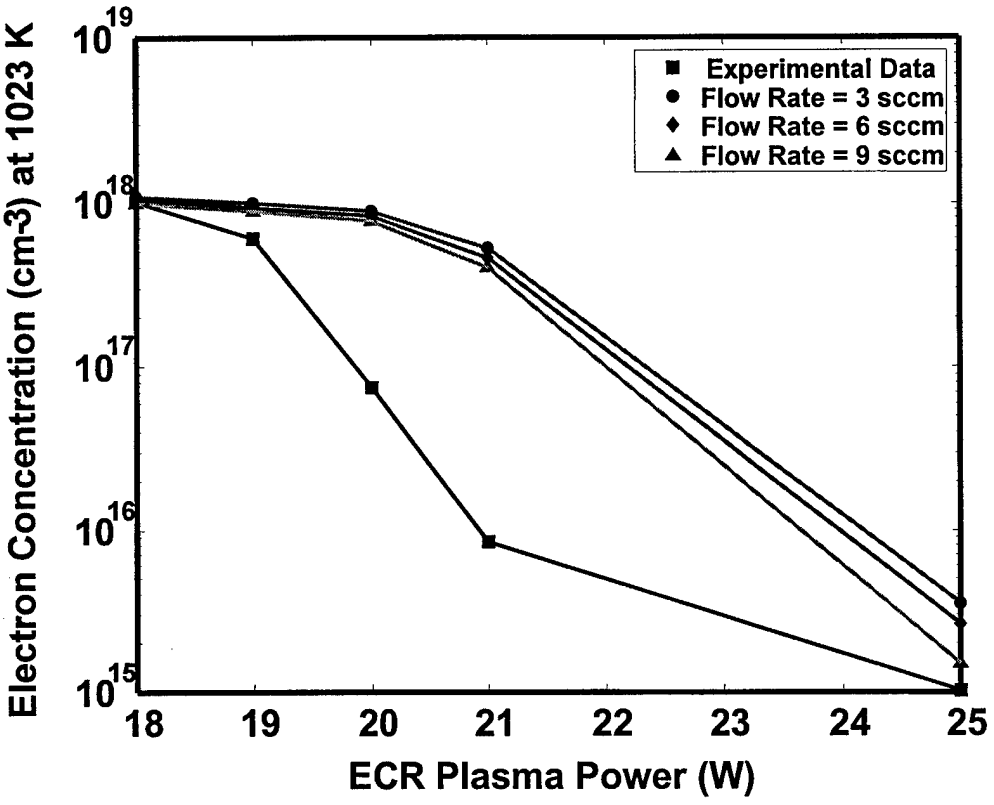

Figure 12. The variation of net electron concentration with the microwave power (W) at 1023 K for various flow rates along with the experimental data [6].

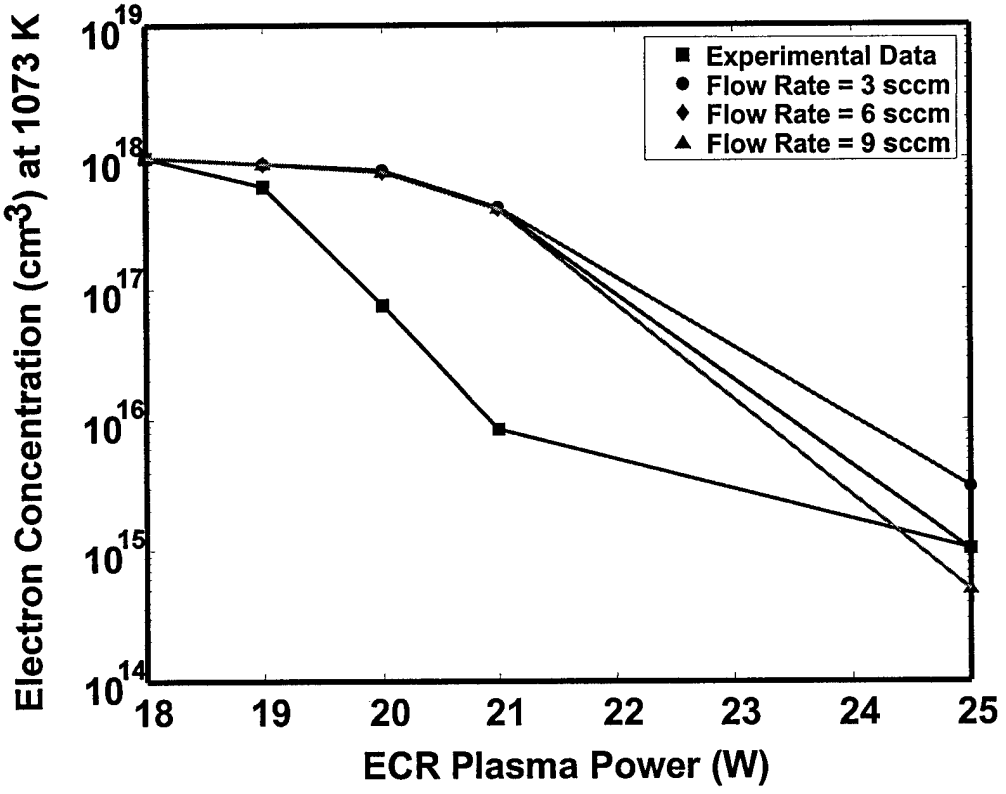

Figure 13. The variation of net electron concentration with the microwave power (W) at 1073 K for various flow rates along with the experimental data [6].

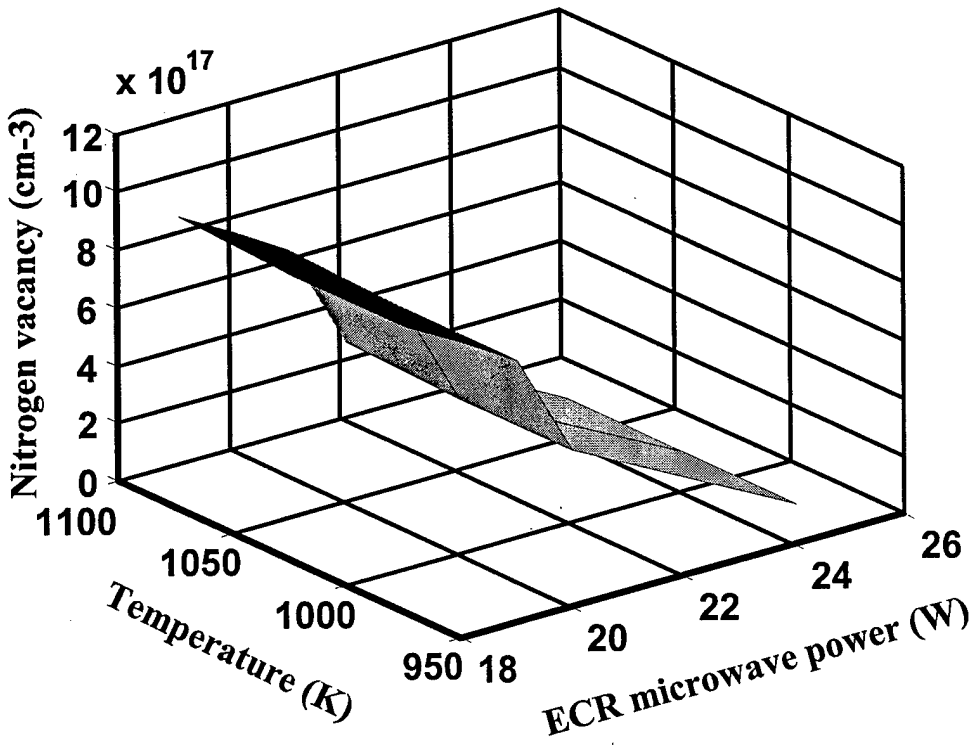

Figure 14. 3-D surface plot of N vacancy concentration $(/cm^3)$ versus temperature (K) and ECR power (W) for a flow rate of 3 $sccm$.

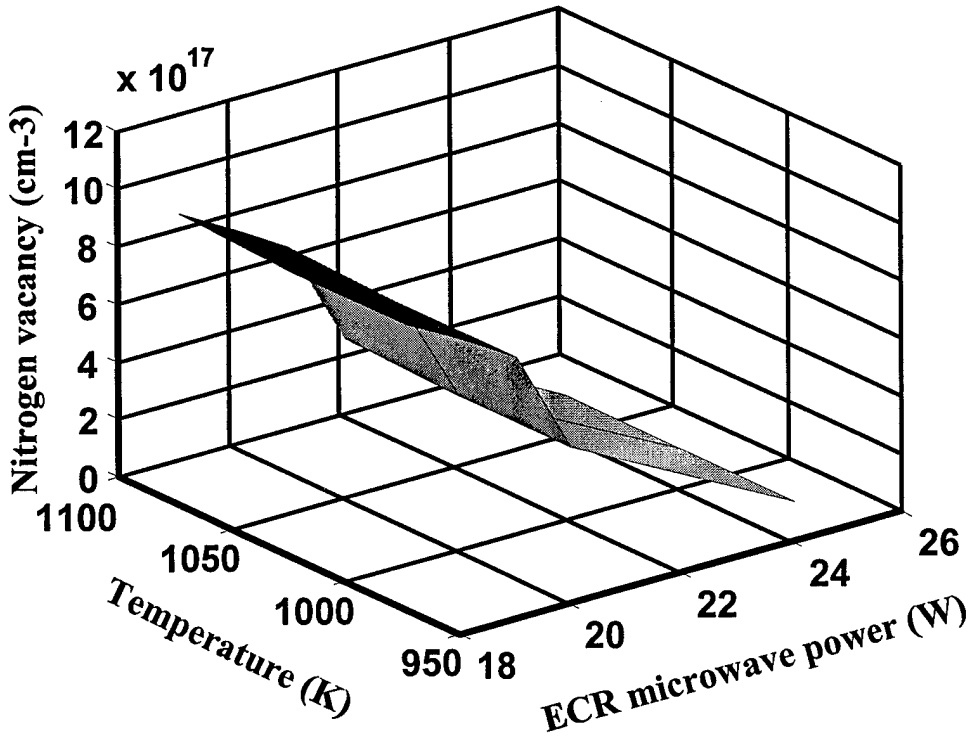

Figure 15. 3-D surface plot of N vacancy concentration $(/cm^3)$ versus temperature (K) and ECR power (W) for a flow rate of 6 *sccm*.

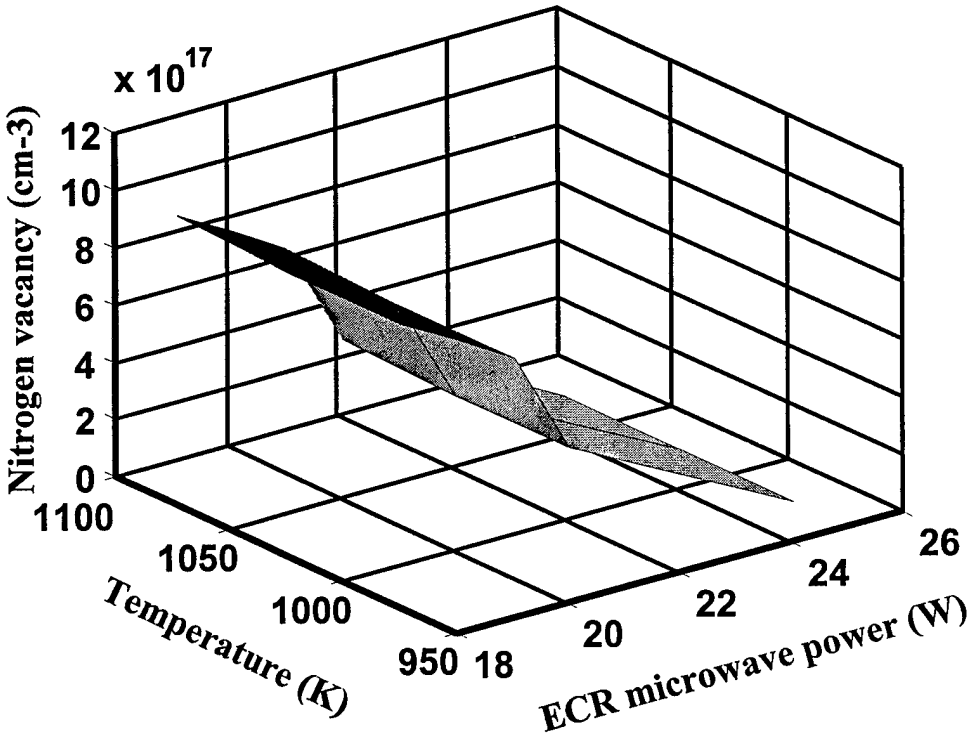

Figure 16. 3-D surface plot of N vacancy concentration $(/cm^3)$ versus temperature (K) and ECR power (W) for a flow rate of 9 $sccm$.

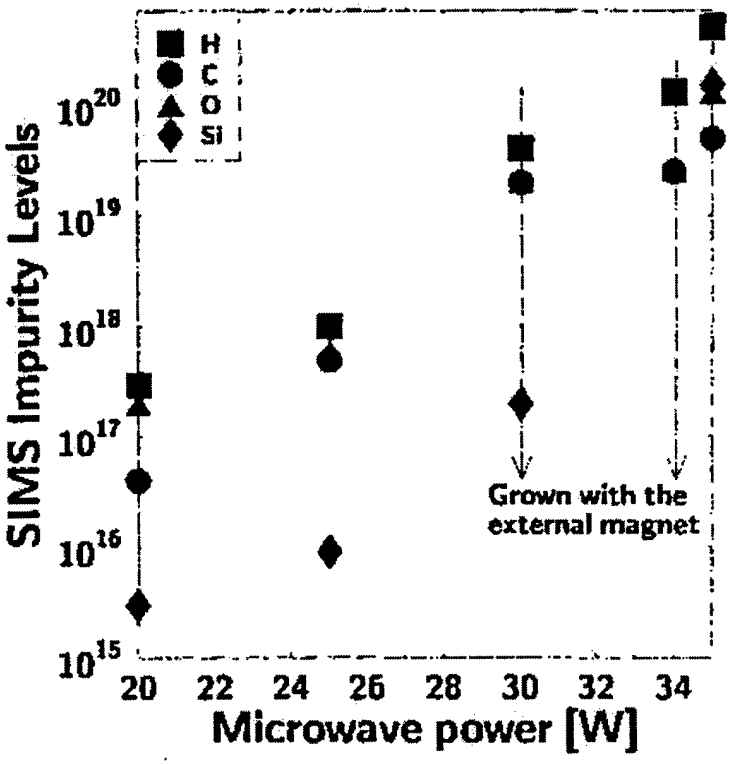

Figure 17. Experimental SIMS impurity levels versus microwave power [6].

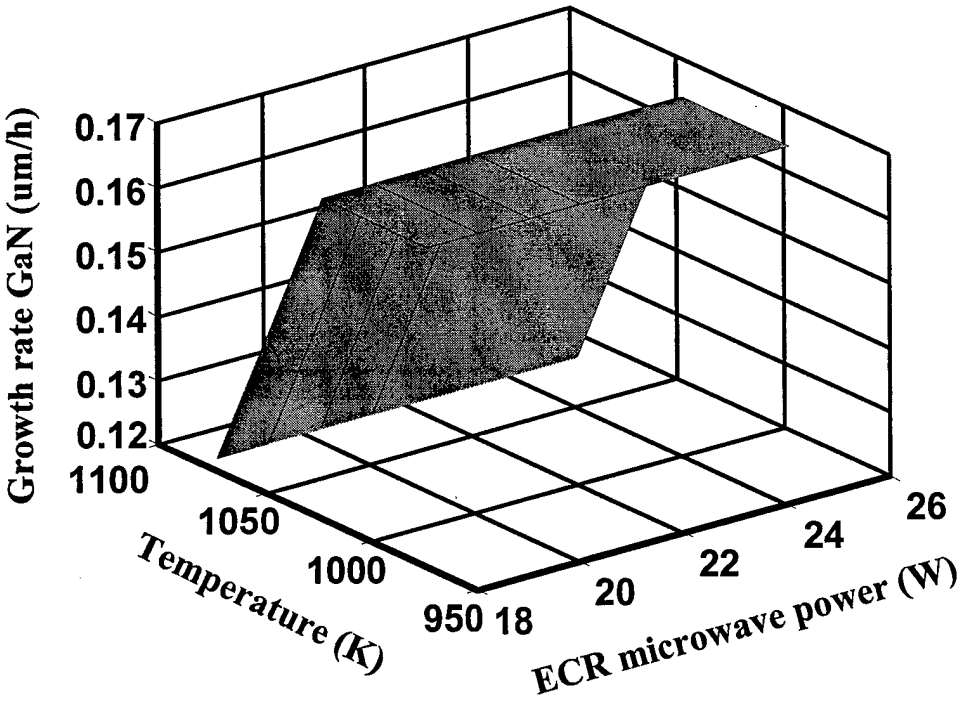

Figure 18. 3-D plot of *GaN* growth rate versus temperature (K) and ECR power (W) for a flow rate 3 *sccm*.

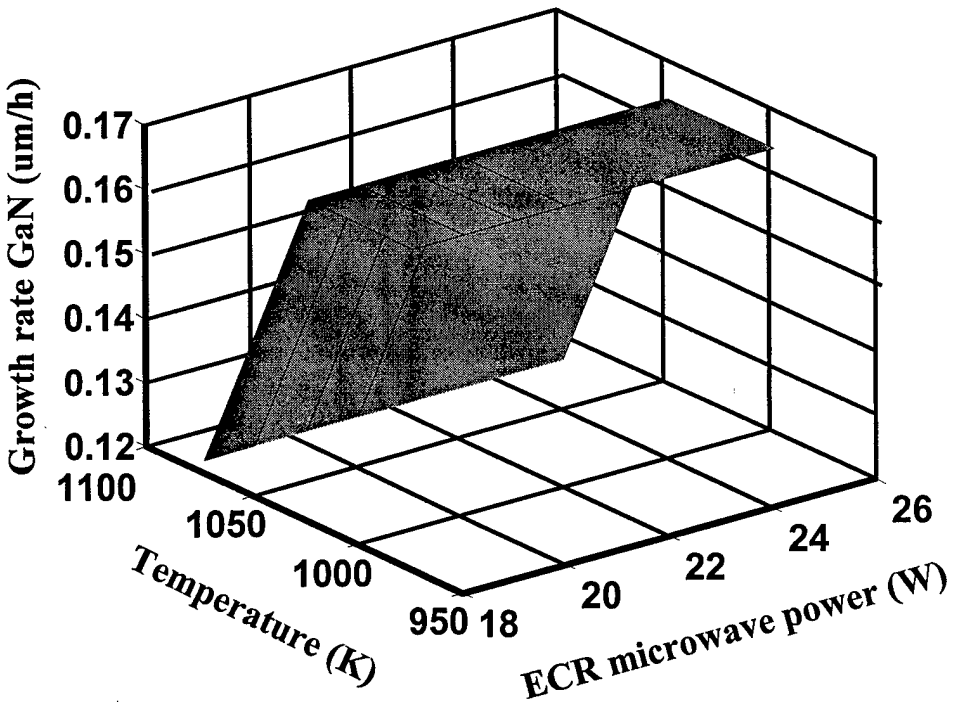

Figure 19. 3-D plot of *GaN* growth rate versus temperature (K) and ECR power (W) for a flow rate 6 *sccm*.

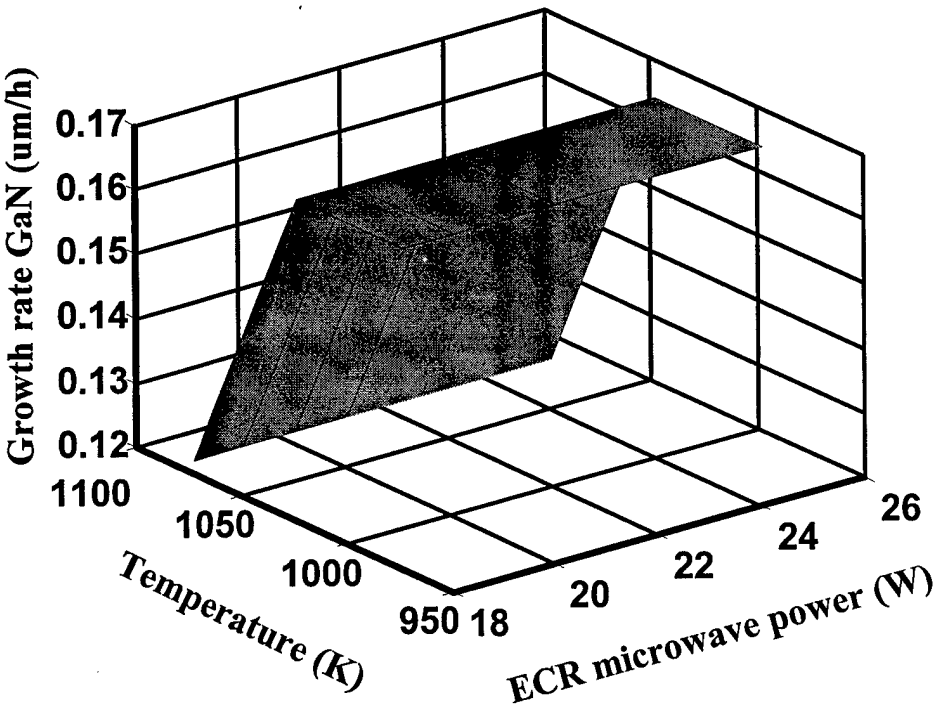

Figure 20. 3-D plot of *GaN* growth rate versus temperature (K) and ECR power (W) for a flow rate 9 *sccm*.

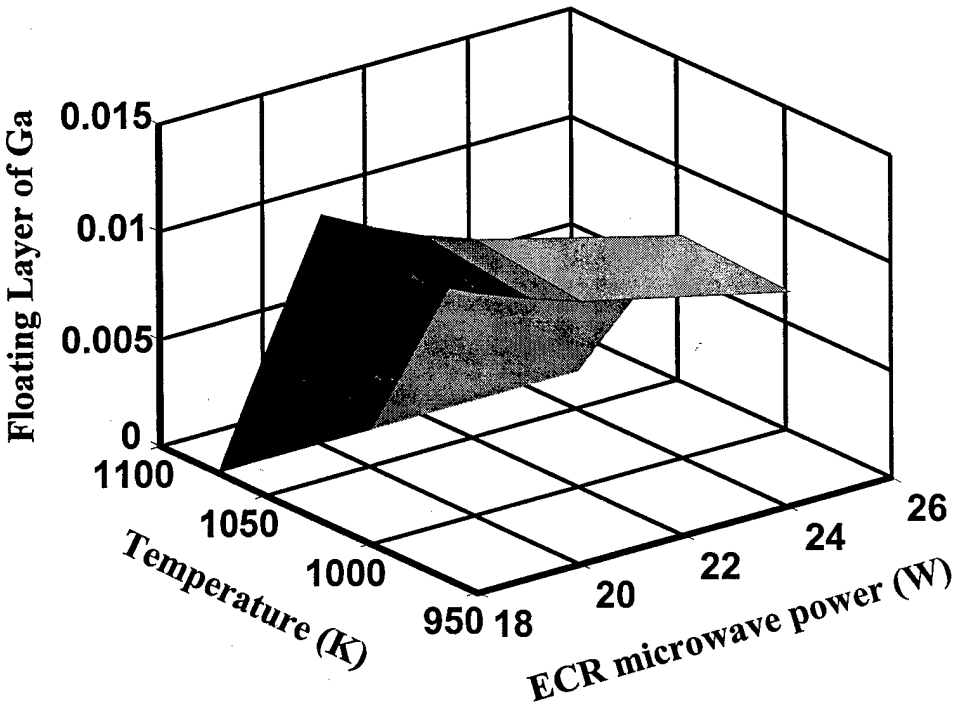

Figure 21. 3-D plot of floating layer of *Ga* coverage versus temperature (K) and ECR power (W) for the case of growth represented in Figure 26.

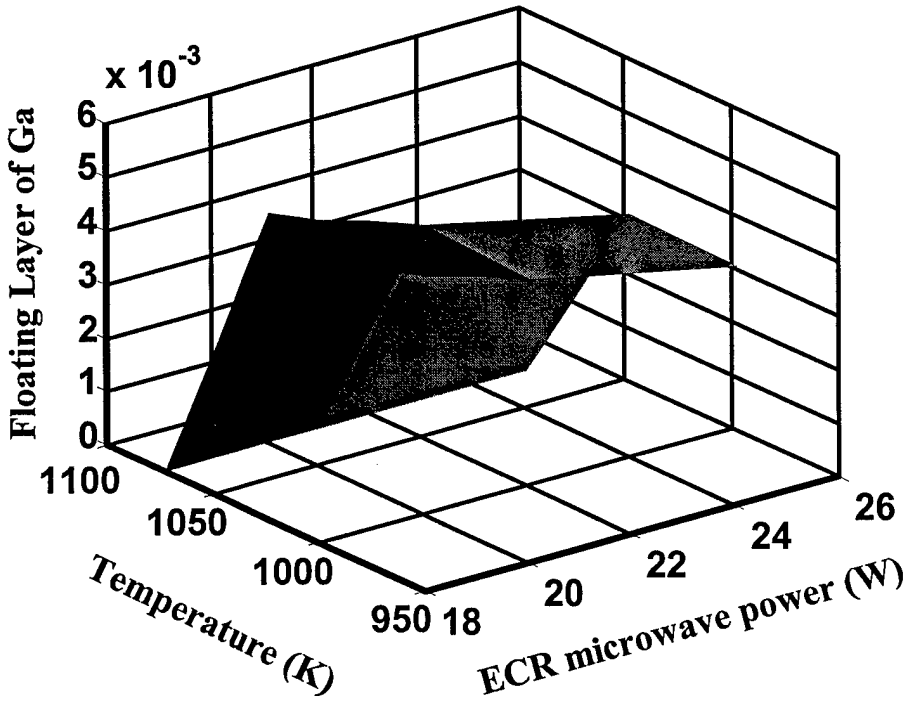

Figure 22. 3-D plot of floating layer of *Ga* coverage versus temperature (K) and ECR power (W) for the case of growth represented in Figure 27.

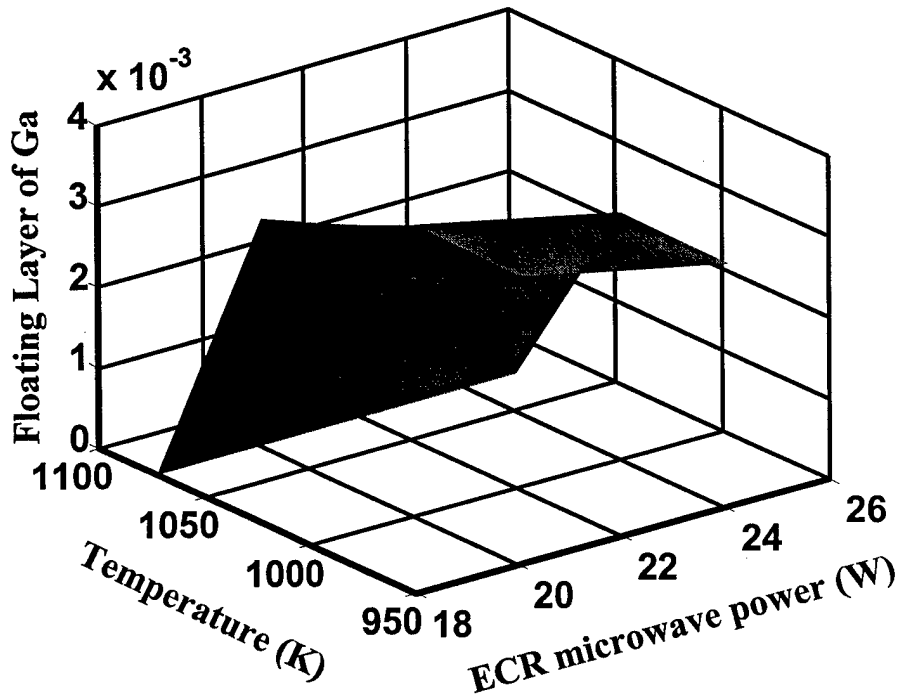

Figure 23. 3-D plot of floating layer of *Ga* coverage versus temperature (K) and ECR power (W) for the case of growth represented in Figure 28.

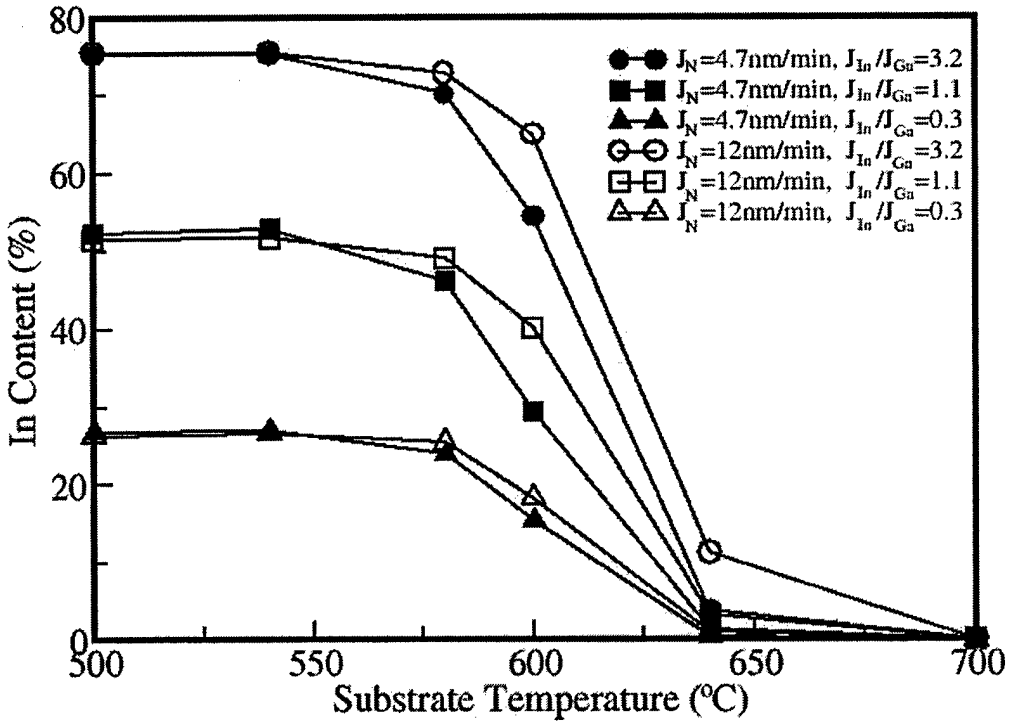

Figure 24. Plots of Indium content in percentage versus the substrate temperature for the nitrogen fluxes of 4.7 *nm/min* and 12 *nm/min*, and various ratios of *In* and *Ga* fluxes.

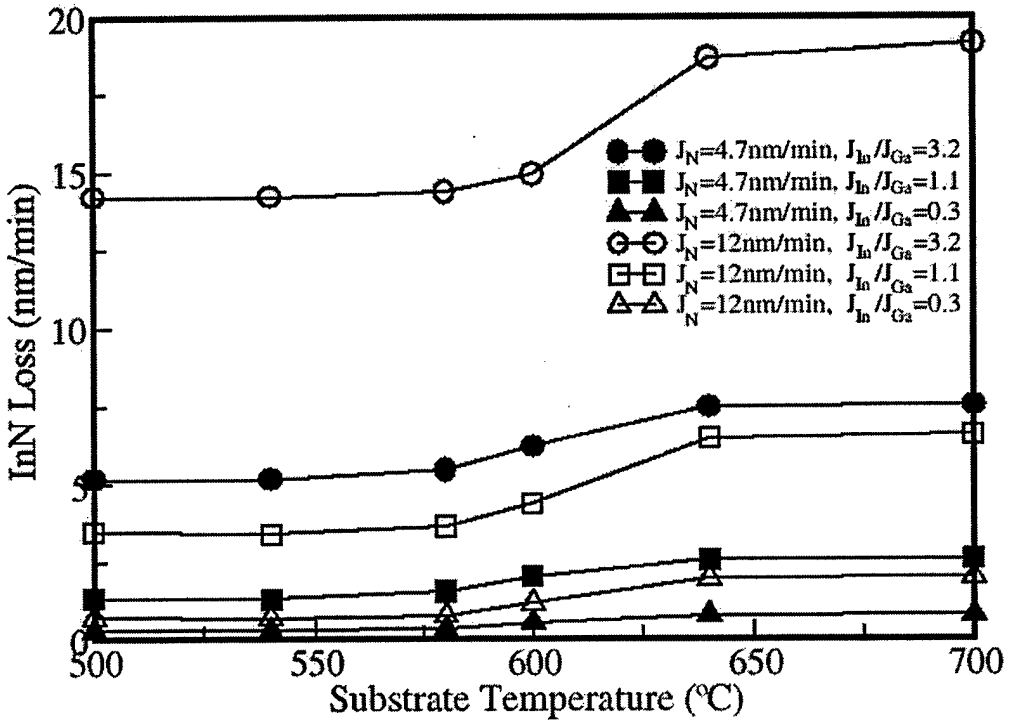

Figure 25. Plots of *InN* loss rate versus temperature for the nitrogen fluxes of 4.7 *nm/min* and 12 *nm/min*, and various ratios of *In* and *Ga* fluxes.

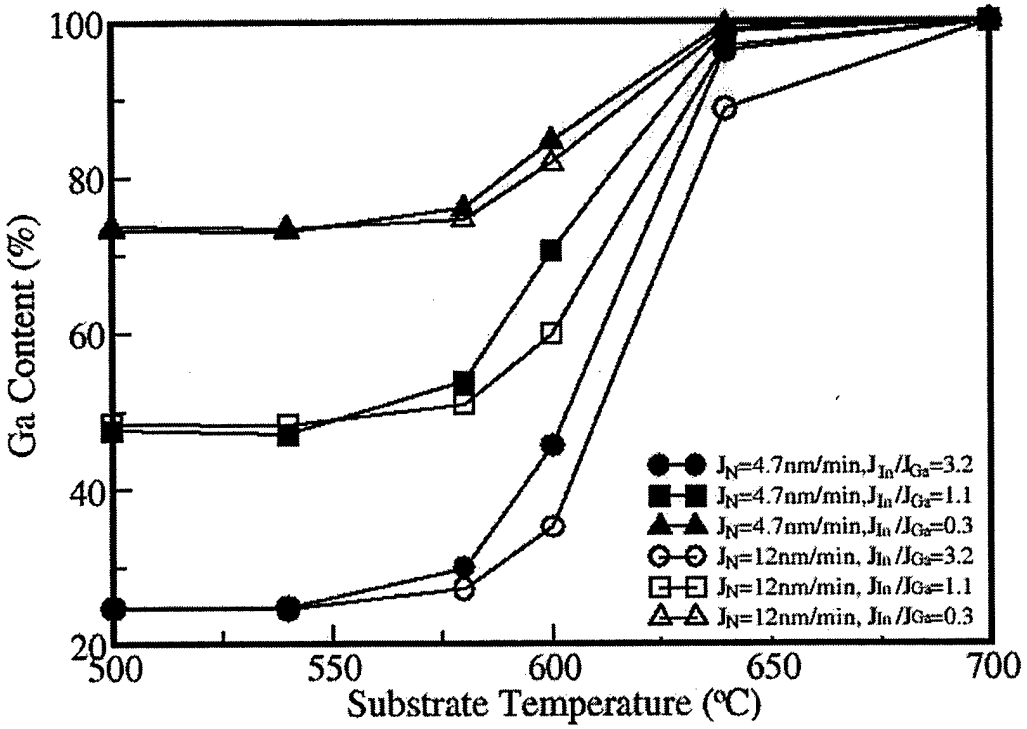

Figure 26. Plots of *Ga* content in percentage versus substrate temperature for the nitrogen fluxes of 4.7 *nm/min* and 12 *nm/min*, and various ratios of *In* and *Ga* fluxes.

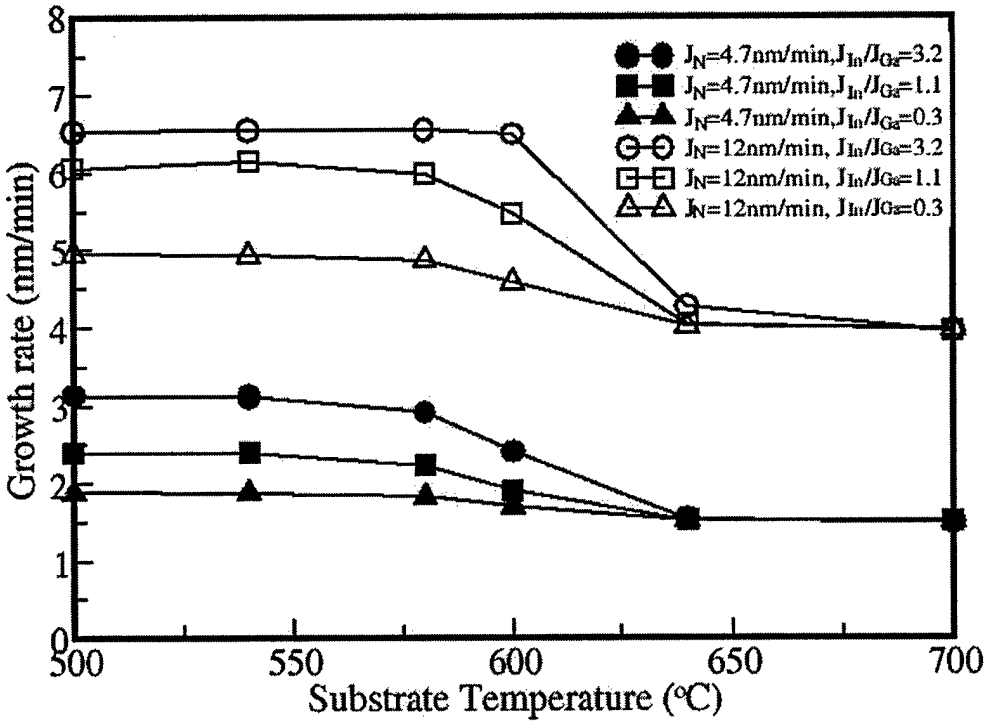

Figure 27. Plots of growth rate versus substrate temperature for the nitrogen fluxes of 4.7 *nm/min* and 12 *nm/min*, and various ratios of *In* and *Ga* fluxes.

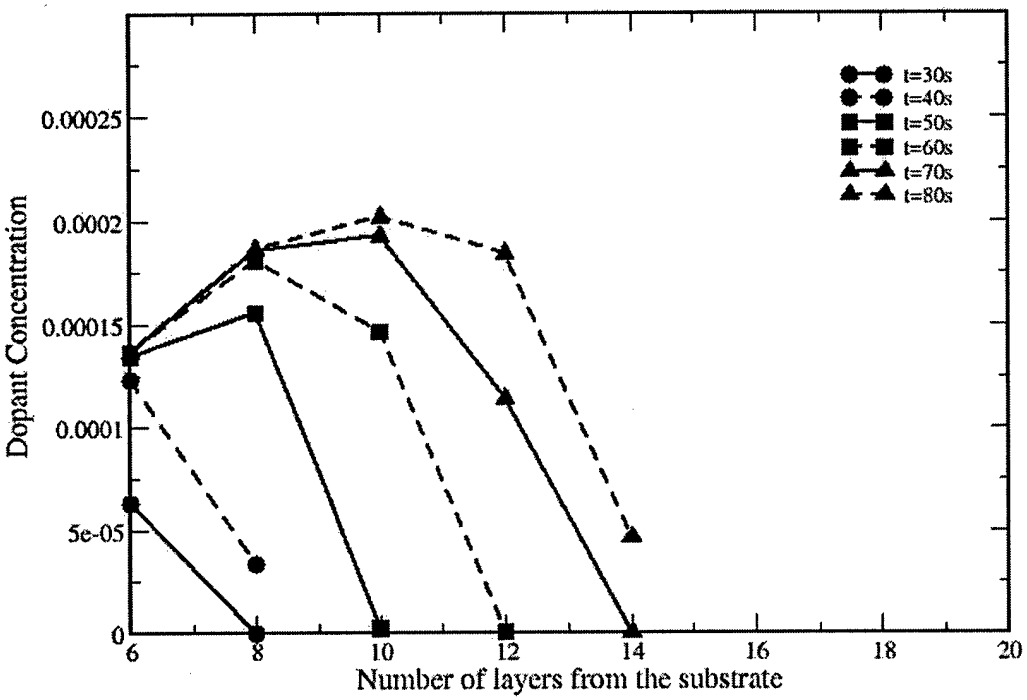

Figure 28. Plot of dopant *Mg* concentration as a function of number of full layers at 600 ^{o}C for various growth times.

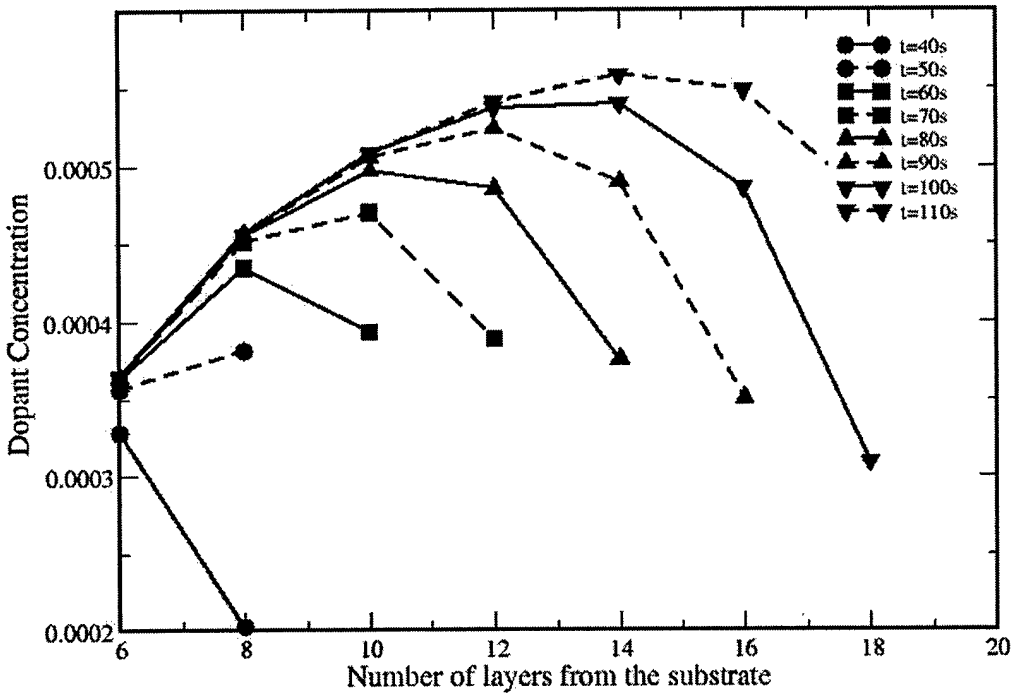

Figure 29. Plot of *Mg* concentration as a function of number of full layers at 680 ^{o}C for various growth times.

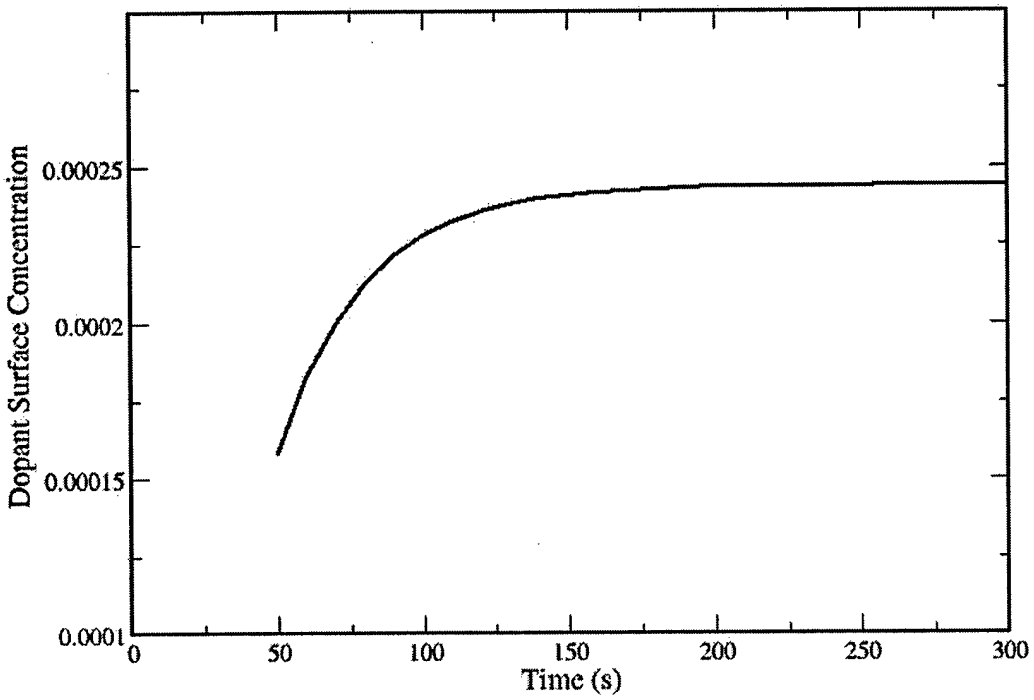

Figure 30. The extrapolated data of the *Mg* surface concentration for increased duration of growth

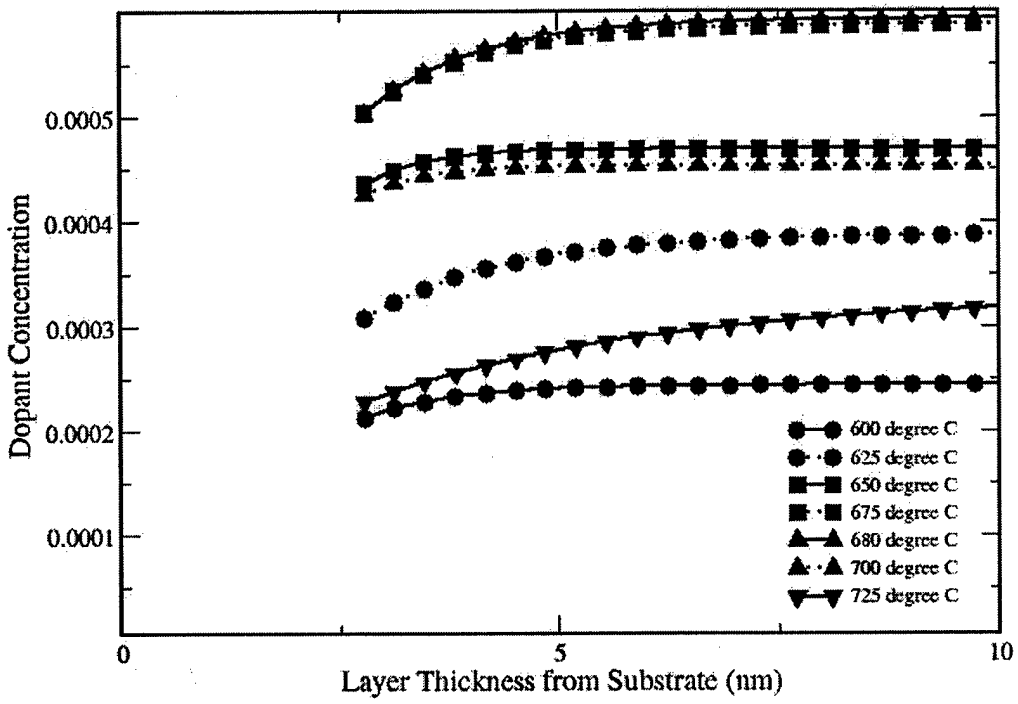

Figure 31. The extrapolated data of *Mg* concentration as a function of layer thickness

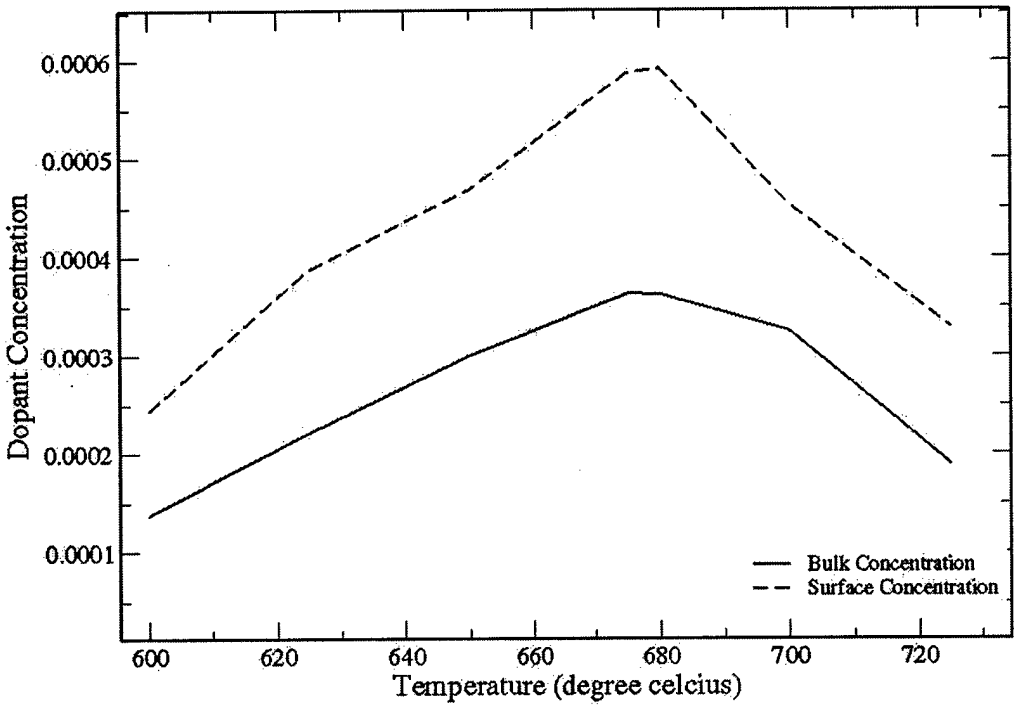

Figure 32. Plot of bulk and extrapolated surface concentration of *Mg* for various growth temperatures

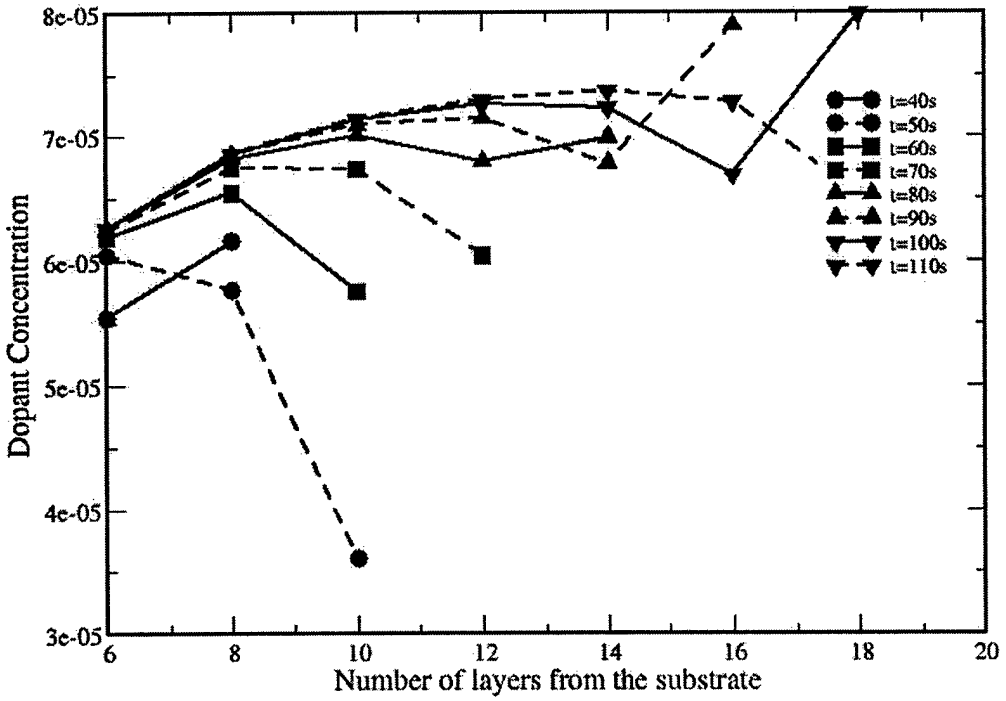

Figure 33. *Mg* concentration versus. layer number at 750 ^{o}C. Note the dopant-depleted zone for longer growth times.

5. OTHER PROJECT INFORMATION

5.1 Current Effort Underway

Currently, we are investigating *In* segregration in *InGaN* MBE growth and its dependence on growth condition. The current research assistant will continue the work and complete her M.S. thesis by December 2002. An undergraduate student will be recruited to work till the end of the project.

5.2 Personnel Supported

Name	Category	Period
Rama Venkat	Professor and P.I.	3/15/99-3/14/03
Golshan Colayni	Graduate Student	6/1/99-8/31/99
Wenning Fu	Graduate Student	6/1/99-12/31/00
Irena Stanley	Graduate Student	8/1/01-2/28/03
Bharathreddy Pemmireddy	Graduate Student	8/1/02-12/31/02
Richard Schofield	Undergraduate Student	1/1/00-5/26/00
Nathan Sipe	Undergraduate Student	5/18/01-12/31/01

5.3 Publications

Presentations

1) Golshan Coleyni and Rama Venkat, *"MBE growth modeling of In desorption in InGaAs/GaAs Compound Semiconductor"* presented in ACCGE 11, Tucson, AZ, August, 1999.
2) Wenning Fu and Rama Venkat, *"Theoretical Study of GaN Growth Using Ammonia"*, presented at 18th North American MBE Conference, Banff, 1999.
3) Wenning Fu and Rama Venkat, *"Theoretical Study of GaN Growth Using ECR Plasma"*, presented at 19th North American MBE Conference, Tempe, AZ, 2000.
4) Irena Stanley, Golshan Coleyni, and Rama Venkat, *"Theoretical Study of In surface kinetics during MBE Growth of InGaAs and InGaN"* presented as a poster

at the XIII International Molecular Beam Epitaxy Conference, San Francisco, CA, September, 2002.

5) Golshan Coleyni and Rama Venkat, *"MBE growth modeling of In desorption in InGaAs/GaAs Compound Semiconductor"* presented in ACCGE 14, Seattle, WA, August, 2002.

6) Irena Stanley and Rama Venkat, *"Mg Segregation in Mg-GaN MBE- A Simulation Investigation"*, submitted to NAMBE 2003, Boulder, CO, 2003.

Master of Science Theses

1) Golshan Coleiny, *"Theoretical Investigation of MBE Growth of InGaAs Semiconductor Compound on GaAs Substrate"*, 1999.

2) Wenning Fu, *"Modeling of GaN Molecular Beam Epitaxy Growth"*, 2000.

3) Irena Stanley, *"Theoretical Study of Segregation Kinetics of In in InGaN and Mg in Mg-GaN Grown by Molecular Beam Epitaxy"*, 2003.

Journal Articles

1) Golshan Coleiny and Rama Venkat, *"MBE growth modeling of In desorption in InGaAs/GaAs Compound Semiconductor"* J. Crys. Growth, vol.211, (2000), p21.
2) Wenning Fu and Rama Venkat, *"Theoretical Study of GaN Growth Using Ammonia"*, J. Vac. Sci. Technol, vol. B18, (2000), p1467.
3) Wenning Fu and Rama Venkat, *"Theoretical Study of GaN Growth Using ECR Plasma"*, J. Vac. Sci. Technol, vol. B19, (2001), p1803.
4) Nathan Sipe, Rama Venkat, *"GaN Growth by Plasma Assisted MBE in the Presence of Low Mg Flux"* MRS Internet Journal of Nitrides, vol.7, 2001.
5) Irena Stanley, Golshan Coleiny, and Rama Venkat, *"Theoretical Study of In surface kinetics during MBE Growth of InGaAs and InGaN"*,J. Crys. Growth, vol. 251, (2003), p23.

6) Golshan Coleyni and Rama Venkat, "MBE growth modeling of In desorption in InGaAs/GaAs Compound Semiconductor", J. Crys. Growth, vol. 250, (2003), p22.

5.4 Interactions

Our success in this area has been limited, even though we tried our best to work with Dr. Mishra's group at UCSB and Dr. Morkoc's group at VCU.

5.5 New Discoveries, Inventions, and Patents

Most of the discoveries have been theoretical ones. They were presented in the journal articles, conference presentations and this report.

5.6 Honors and Awards

None.